2009

Optimization of solid oxide fuel cell interconnect design

Krishna C. Pulagam
University of Nevada Las Vegas

OPTIMIZATION OF SOLID OXIDE FUEL CELL

INTERCONNECT DESIGN

by

Krishna C Pulagam

Bachelor of Technology in Mechanical Engineering
Acharya Nagarjuna University, India
2007

A thesis submitted in partial fulfillment
of the requirements for the

Master of Science Degree in Mechanical Engineering
Department of Mechanical Engineering
Howard R. Hughes College of Engineering

Graduate College
University of Nevada, Las Vegas
December 2009

UNIVERSITY OF NEVADA LAS VEGAS

THE GRADUATE COLLEGE

We recommend that the thesis prepared under our supervision by

Krishna C Pulagam

entitled

Optimization of Solid Oxide Fuel Cell Interconnect Design

be accepted in partial fulfillment of the requirements for the degree of

Master of Science
Mechanical Engineering

Yitung Chen, Committee Chair

Robert Boehm, Committee Member

Jianhu Nie, Committee Member

Yahia Bagzhouz, Graduate Faculty Representative

Ronald Smith, Ph. D., Vice President for Research and Graduate Studies
and Dean of the Graduate College

December 2009

ABSTRACT

Optimization of Solid Oxide Fuel Cell Interconnect Design

by

Krishna C Pulagam

Dr. Yitung Chen, Examination Committee Chair
Professor of Department of Mechanical Engineering
University of Nevada, Las Vegas

Performance of solid oxide fuel cells (SOFC) is dependent of a set of complex physical and chemical processes occurring simultaneously. Interconnect for SOFC is important as it provides electrical connection between anode of one individual cell to the cathode of neighboring one. It also acts as a physical barrier to protect the air electrode material from the reducing environment of the fuel on the fuel electrode side, and it equally prevents the fuel electrode material from contacting with oxidizing atmosphere of the oxidant electrode side. A three-dimensional numerical model has been developed to evaluate the SOFC including the current collector, rectangular duct gas flow channels, gas diffusion electrodes and electrolyte layer. This model takes into account the hydrodynamic multi-component fluid flow and heat transfer analysis. Numerical results from the developed model using finite element method (COMSOL®) show that the predicted polarization curve is in very good agreement with the published data. Simulations were also performed for different interconnect design cases obtained by varying electrode/interconnect contact area using finite volume method (Fluent®) to investigate the thermal and hydrodynamic behavior and finite element method (COMSOL®) to investigate the electrical performance. The optimization is carried out by considering 25% interconnect contact area as the design criteria for maximum

temperature gradient limitation. The best interconnect design with 60% interconnect contact area has been chosen which shows good thermal behavior with considerable power output among the different design cases. Simulations show a decreasing power density and reduction of temperature gradient for an increasing contact area. Parametric studies of the fuel cell for different mass flows, hydraulic diameters and interconnect material properties for optimized design have also been performed. Results reveal that the flow rate will have minor impact on the electrical performance compared to the effect of material properties. Strontium doped $LaCrO_3$ has shown better performance than calcium or magnesium doped $LaCrO_3$. Decreasing the hydraulic diameter improves the mass transport situation along the length of the flow channel.

TABLE OF CONTENTS

LIST OF FIGURES

LIST OF TABLES

NOMENCLATURE

a	Activity
A	Area (m^2)
ASR	Area specific resistance (Ω-m^2)
b	Tafel slop
c	Molar concentration (mol/m^3)
c_t	Total concentration of the species (mol/m^3)
c_{ref}	Reference concentration (mol/m^3)
D_{ij}	Binary diffusivity (m^2/s)
D_{ij}^{eff}	Effective diffusivity (m^2/s)
D_h	Hydraulic diameter (m)
E, E_{thermo}	Thermodynamic ideal voltage (V)
E^0	Standard potential under 25 ^oC, 1 atm (V)
F	Faraday constant (96487 C/mol)
f	Friction factor
$\Delta \hat{g}$	Molar Gibbs free energy (kJ/mol)
h	Enthalpy (J/mol)
I , I_{ref}	Current (A) and reference current (A/m^2)
I	Identity matrix
i	Current (A)
$\hat{i}$	Current flux vector

i_{ct}	Charge transfer current density (A/m^2)
i_{ion}	Ionic current (A)
i_{elec}	Electronic current (A)
$j_{o,a}$	Anode exchange current density (A/m^2)
$j_{o.c}$	Cathode exchange current density (A/m^2)
j	Current density (A/m^2)
j_o	Exchange current density (A/m^2)
j_L	Limiting current density (A/m^2)
k	Permeability (m^2)
k_d	Reference diffusivity (m^2/s)
k_s	Electrical conductivity (S/m)
k^{eff}	Effective heat conductivity (W/m-K)
M_{w,H_2}	Molecular weight of hydrogen (g/mol)
M_{w,H_2O}	Molecular weight of water (g/mol)
M_{w,O_2}	Molecule weight of oxygen (g/mol)
n	Number of electrons transferred in the reaction
$\hat{n}$	Unit vector
P	Pressure (Pa or atm)
Q	Mass source term
R	Ideal gas constant (8.314 J/mol-K)
R	Electric resistance (Ω)

R_i	Reaction source term (g/m^2-s)
Re	Reynolds number
S	Mass sink or source rate
S_T	Heat source (W/m^3)
S_a	Specific surface area (m^2)
T	Absolute temperature (K)
U	Velocity vector
u	Velocity (m/s)
$\bar{u}$	Mean velocity (m/s)
V , V_{cell}	Cell voltage output (V)
V_{pol}	Polarization voltage (V)
w_i	Weight fraction of species i
X , x_i	Mass fraction and molar fraction of species i
α	Charge transfer coefficient
α^*	Aspect ratio
Δ	Denotes change in quantity
ε	Porosity
σ	Electric conductivity (S/m)
ϕ_{elec} , ϕ_{ion}	Electronic and ionic potential (V)
$\Delta\phi_{eq}$	Equilibrium potential difference (V)
η	Overvoltage (V)
η_{act}	Activation overvoltage (V)

η_{ohmic}	Ohmic overvoltage (V)
η_{conc}	Concentration overvoltage (V)
ρ	Density (kg/m^3)
ν	Stoichiometric coefficient
ς	Shear stress tensor
μ	Fluid dynamic viscosity (kg/m-s)

ACKNOWLEDGEMENT

I would like to expresses my sincere gratitude and profound appreciation to my honorific advisor, Dr. Yitung Chen, who was abundantly helpful and offered invaluable assistance, support and guidance with his experience and knowledge. Without his motivation, encouragement and immense patience, this thesis would not have been completed or written. I am also greatly thankful to Dr. Jianhu Nie for his assistance, generosity and advice throughout this study.

I would like to thank all the professors who taught me, to complete my course work which laid strong fundamentals for the completion of my thesis work.

I am also thankful and appreciate Dr. Robert F Boehm and Dr. Yahia Baghzouz for their time to review my thesis and participation as defense committee members.

I am very much thankful for my parents Mr. P.R.K.Murthy and Mrs. Anasuya, my sister Lavanya for their unconditional support and selfless love throughout my life. Finally, I extend my love to all my friends who cheered me up and made me feel homelike, away from home.

CHAPTER 1

INTRODUCTION

1.1 What is a Fuel Cell

A fuel cell is an electrochemical conversion device. It produces electricity from fuel (on the anode side) and an oxidant (on the cathode side), which react in the presence of an electrolyte. The reactants flow into the cell, and the reaction products flow out of it, while the electrolyte remains within it. Fuel cells can operate virtually continuously as long as the necessary reactants and products flows are maintained [1].

Fuel cells are different from electrochemical cell batteries in that they consume reactant from an external source, which must be replenished– a thermodynamically open system. By contrast, batteries store electrical energy chemically and hence represent a thermodynamically closed system.

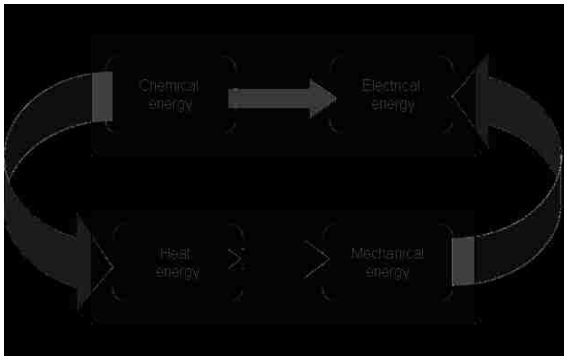

Fig.1.1 Comparison between fuel cell, battery and engine

As shown in Fig.1.1 unlike combustion engines a fuel cell produces electricity directly from chemical energy and is far more efficient. Fuel cells can be all solid state and mechanically ideal, meaning no moving parts. This yields the potential for

highly reliable and long lasting systems. A lack of moving parts also means that fuel cells are silent. Also, undesirable products such as NO_x, SO_x and particulate emissions are virtually zero.

Apart from the advantages, fuel cells also possess some serious disadvantages. Cost represents a major barrier to fuel cell implementation, because of prohibitive costs; fuel cell technology is currently only economically competitive in a few highly specialized applications [2]. Power density is another significant limitation. Although fuel cell power densities have improved dramatically over the past decades, further improvements are required if fuel cells are to compete in portable and automotive applications. Fuel availability and storage pose further problems, as fuel cells works best on hydrogen gas, a fuel that is not widely available, has a low volumetric energy density, and is difficult to store. Alternative fuels are difficult to use directly and usually require reforming. These problems can reduce fuel cell performance and increase the requirements for ancillary equipments. Additional fuel cell limitations include operational temperature compatibility concerns, susceptibility to environmental poisons, and durability under start-stop cycling [1].

1.2 Global View

Although fuel cells represent less than half of one percent of the application markets for power of any type, including portable power (where they compete against batteries and portable generators), stationary power (where they compete against the electric power grid), or vehicle power (where they compete against the internal combustion engine), it is growing at a faster speed. Prices have yet to significantly

decrease but are expected to fall as mass production ramps up. Fuel cell manufacturers receive government support through subsidies as well as coordinated research and development. Limited mass production of fuel cell vehicles is not expected to begin before 2015, although many manufacturers will produce about 100 fuel cell vehicles a year for fleet demonstrations. Development of hydrogen fueling stations for these vehicles continues at a rate of about two to four a month worldwide. More than $500 billion worth of hydrogen fueling stations will eventually be needed to compete with the world-wide gasoline infrastructure [3].

The demand for eco-friendly low-maintenance energy storage solutions with long life spans has resulted in the creation of a $193.64 million market for stationary fuel cells in the world. The global stationary fuel cells market, largely dominated by the US, Japan and South Korea, is expected to expand with increasing interest in other nations. While the need to replace lead acid batteries with a non-toxic-substance-based storage solution drives fuel cells uptake in developed markets such as the US and Japan, the demand for low-maintenance long back-up storage solutions drives technology adoption in developing nations. Regulatory push for clean technology by the Obama administration is expected to boost the US stationary fuel cells market. Volume sales and R&D initiatives resulting from increased investment due to regulatory support are expected to accelerate price fall and commercialization of fuel cells. Nevertheless, mass adoption of fuel cells is expected to be prevented by the lack of infrastructure for supporting market development and, to certain extent, by technological limitations of the technology [4].

The lure of fuel cells is the promise to be one of the most ubiquitous products of the 21st century. Fuel cells can compete with batteries, the internal combustion engine and the power grid. Hydrogen can compete with any fuel now produced and cause no pollution but its price is higher than gasoline or natural gas because it is difficult to transport and store. Nanotechnologies will provide the technological keys that enable fuel cells and hydrogen as a fuel to become competitive and commonplace.

According to a soon-to-be-released report from Interactive Risk Attributable Program (IRAP), Fuel Cells, Hydrogen Energy and Related Nanotechnology—A Global Industry and Market Analysis, the fuel cell and hydrogen energy industry is highly fragmented. Worldwide about 3870 organizations are involved in fuel cells, hydrogen energy and related nanotechnology and spent an estimated $8.4 billion in 2008. This market is estimated at $8.8 billion in 2009 and expected to increase to $14 billion by 2014, with a compound average growth rate of 9.6%. More than 2180 organizations are involved in nanotechnology related to fuel cells and hydrogen energy and will spend a total of $4.7 billion for fuel cells and hydrogen energy incorporating nanotechnology. Of that $4.7 billion, about $2 billion in 2008 represents the value of nanotechnology for fuel cells and hydrogen energy separate from all other expenditures [3].

1.3 Fundamentals of Fuel Cell

Fuel cell is an electrochemical device which converts chemical energy directly to electrical energy without intermediate heat step. Fig.1.2 shows the one-dimensional cross sectional view of planar SOFC. Using this figure as a map, we will now embark on a

brief journey through the major steps involved in producing electricity in a fuel cell. Sequentially, as shown in Fig.1.2, these steps are as follows:

1. Reactant delivery (transport) into the fuel cell
2. Electrochemical reaction
3. Ionic conduction through the electrolyte and electron conduction through the external circuit
4. Product removal from the fuel cell

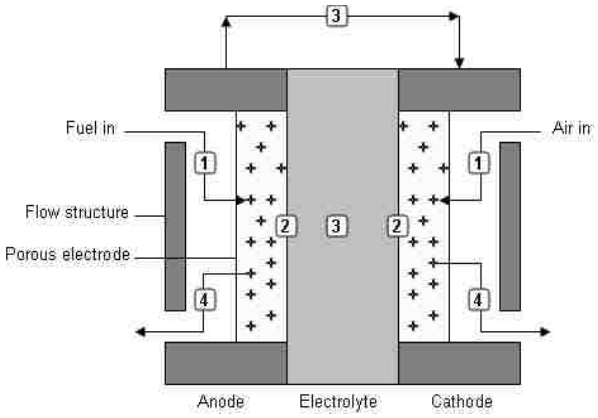

Fig. 1.2 Cross-section of fuel cell illustrating major steps in electrochemical generation of electricity

The electrochemical reactions (reduction and oxidization) taking place at the electrode can be expressed as:

$$aA \leftrightarrow cC + ne^{-} \quad (oxidation)$$
$$bB + ne^{-} \leftrightarrow dD \quad (reduction)$$
$$aA + bB \leftrightarrow cC + dD \quad (net\ reaction)$$

As all chemical reactions involve electrons, harnessing these electrons defines the efficiency of fuel cell. Fuel cells received serious attention from last decade for their high efficiency in the field of renewable energy sources. An ideal fuel cell would supply any

amount of current, while maintaining a constant voltage determined by thermodynamics. But in practice, however, the actual voltage output of a real fuel cell is less than the ideal thermodynamically predicted voltage (E_{thermo}) due to irreversible losses. There are three major types of fuel cell losses, which give a fuel cell $j-V$ curve its characteristic shape.

- Activation loss η_{act} (loss due to electrochemical reaction)

  An activation barrier impedes the conversion of reactants to products and vice versa. A portion of the fuel cell voltage is sacrificed to lower the activation barrier, thus increasing the rate at which reactants are converted into products and the current density (j) generated by the reaction. The sacrificed (lost) voltage is known as activation overvoltage η_{act}. The relationship between the current density output and the activation overvoltage is exponential as shown in Fig.1.3. It is described by the Butler-Volmer equation:

$$j = j_0(e^{\alpha nF\eta_{act}/(RT)} - e^{-(1-\alpha)nF\eta_{act}/(RT)}) \tag{1-1}$$

  Fuel cells are usually operated at relatively high current densities (high activation overvoltage). At high activation overvoltage, fuel cell kinetics can be approximated by a simplified version of the Butler-Volmer equation: $j = j_0 e^{\alpha nF\eta_{act}/(RT)}$. In a generalized logarithmic form, this is known as the Tafel equation

$$\eta_{act} = a + b\log j \tag{1-2}$$

  where b is the Tafel slope, α is the transfer coefficient and j_0 is the reference exchange current density.

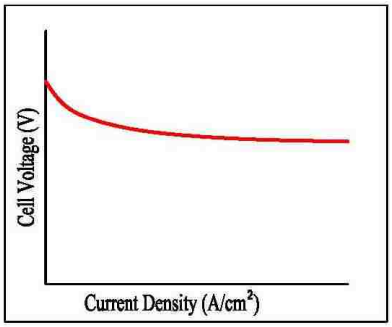

Fig.1.3 Activation loss

- Ohmic loss η_{ohmic} (loss due to ionic and electronic conduction)

Charge transport in fuel cells is predominantly driven by a voltage gradient. This charge transport process is known as conduction. The voltage that is expended to drive conductive charge transport represents a loss to fuel cell performance. Known as the ohmic overvoltage, this loss generally obeys Ohm's law of conduction and it varies linearly as shown in Fig.1.4.

$$\eta_{ohmic} = j\left(ASR_{ohmic}\right) \tag{1-3}$$

where j is the current density and ASR_{ohmic} is the area specific resistance which includes the resistance from electrodes, electrolyte, interconnects and so on. However, it is usually dominated by the electrolyte resistance.

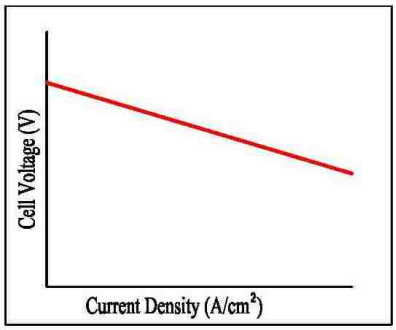

Fig. 1.4 Ohmic loss

- Concentration loss η_{conc} (loss due to mass transport)

Mass transport governs the supply and removal of reactants and products in a fuel cell. Mass transport in fuel cell electrodes is typically dominated by diffusion and in fuel cell flow structure is typically dominated by convection. Diffusive transport limitations in the electrode lead to a limiting current density j_L. The limiting current density corresponds to the point where the reactant concentration falls to zero in the fuel cell catalyst layer. A fuel cell can never sustain a current density higher than j_L. Reactant depletion affects both the Nernstian cell voltage and the kinetic reaction rate. Depletion leads to similar loss in both cases. This "concentration loss" can be generalized as and its characteristic plot is shown in Fig.1.5.

$$\eta_{conc} = c[\, j_L /(j_L - j)] \tag{1-4}$$

$$j_L = nFD^{eff}\frac{c_R^o}{\delta} \tag{1-5}$$

where c is a constant that depends on the geometry and mass transport properties of the fuel cell, D^{eff} is the effective reactant diffusivity (m^2/s), c_R^o is the bulk (flow channel) reactant concentration (mol/m^3), δ is the electrode (diffusion layer) thickness (m).

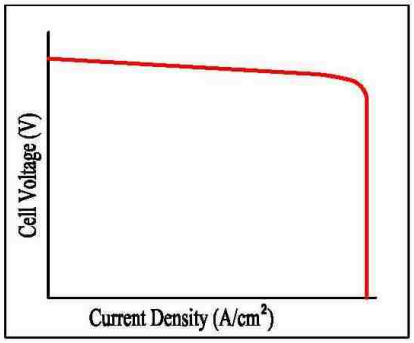

Fig.1.5 Concentration loss

Fig.1.6 shows the characteristic polarization curve for a single fuel cell. Here it is evident that actually as the current density increases the voltage of the fuel cell decreases. The fuel cell polarization curve can be divided into three regions where each of the major losses dominate in their respective regions. In Region I, the activation polarization loss is significant, which is controlled by the electrode kinetics of the reaction; in Region II, which is generally the fuel cell operating region, the ohmic loss dominates, and the ohmic loss is proportional to the current density. This is due to the cell resistance of the ions in electrolyte; in Region III, where the current density is very high, the mass transport of reactants to the electrode reaches its limit, and then the concentration limit loss becomes the predominant factor.

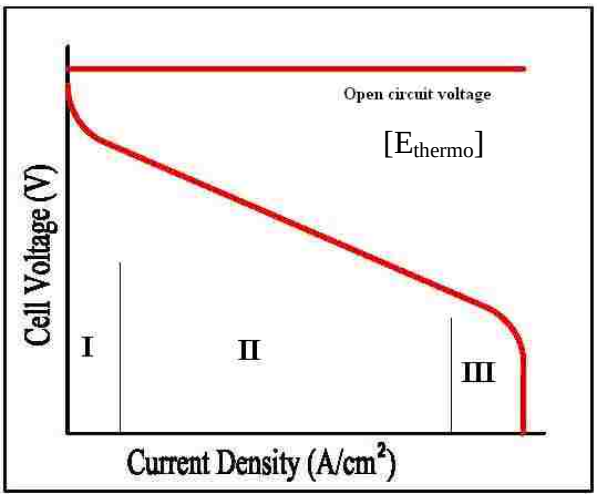

Fig.1.6 Fuel cell polarization curve

The real voltage output (V) for a fuel cell can thus be written by starting with thermodynamically predicted voltage output of the fuel cell and then subtracting the voltage drop to the various losses:

$$V = E_{thermo} - \eta_{act} - \eta_{ohmic} - \eta_{conc} \tag{1-6}$$

The reversible voltage of a fuel cell, E_{thermo} or E, is related to the molar Gibbs free energy by

$$\Delta \hat{g} = -nFE \tag{1-7}$$

Generally, the Nernst equation describes how E varies with reactant/product activities:

$$E = E^0 - \frac{RT}{nF} \ln \frac{\prod a^{vi}{}_{products}}{\prod a^{vi}{}_{\text{reactants}}} \tag{1-8}$$

where F is the Faraday constant (96487 C/mol), E^0 is the standard potential under the standard state (25^{o}C and 1 atm), R is gas constant, T is operating temperature (K), n is number of moles of electrons and a is the species activity.

1.4 Types of Fuel Cells

Depending upon the nature of the electrolyte, the fuel type and the type of application fuel cells are classified into five major types.

- Alkaline fuel cells (AFC)
- Phosphoric acid fuel cell (PAFC)
- Molten carbonate fuel cells (MCFC)
- Direct Methanol fuel cell (DMFC)
- Solid oxide fuel cells (SOFC)

Alkaline fuel cells use a solution of potassium hydroxide in water as the electrolyte and can use a variety of non-precious metals as a catalyst at the anode and cathode. High-temperature AFCs operate at temperatures between 100ºC and 250ºC (212ºF and 482ºF). However, more-recent AFC designs operate at lower temperatures of

roughly 23ºC to 70ºC (74ºF to 158ºF) [2]. AFCs are high-performance fuel cells due to the rate at which chemical reactions take place in the cell. The disadvantage of this fuel cell type is that it is easily poisoned by carbon dioxide (CO_2). In fact, even the small amount of CO_2 in the air can affect the cell's operation, making it necessary to purify both the hydrogen and oxygen used in the cell.

Phosphoric acid fuel cells use liquid phosphoric acid as an electrolyte—the acid is contained in a Teflon-bonded silicon carbide matrix—and porous carbon electrodes containing a platinum catalyst. This type of fuel cell is typically used for stationary power generation, but some PAFCs have been used to power large vehicles such as city buses. They are 85 percent efficient when used for the cogeneration of electricity and heat, but less efficient at generating electricity alone [2].

Polymer electrolyte membrane (PEM) fuel cells—also called proton exchange membrane fuel cells—deliver high power density and offer the advantages of low weight and volume, compared to other fuel cells. PEM fuel cells use a solid polymer as an electrolyte and porous carbon electrodes containing a platinum catalyst [1]. They need only hydrogen, oxygen from the air, and water to operate and do not require corrosive fluids like some fuel cells. They are typically fueled with pure hydrogen supplied from storage tanks or onboard reformers. Polymer electrolyte membrane fuel cells operate at relatively low temperatures, around 80°C (176°F). Low temperature operation allows them to start quickly (less warm-up time) and results in less wear on system components, resulting in better durability. However, it requires that a noble-metal catalyst (typically platinum) be used to separate the hydrogen's electrons and protons, adding to system cost. PEM fuel cells are used primarily for transportation applications and some stationary

applications. Due to their fast startup time, low sensitivity to orientation, and favorable power-to-weight ratio, PEM fuel cells are particularly suitable for use in passenger vehicles, such as cars and buses [2].

MCFCs are high-temperature fuel cells that use an electrolyte composed of a molten carbonate salt mixture suspended in a porous, chemically inert ceramic lithium aluminum oxide ($LiAlO_2$) matrix. Since they operate at extremely high temperatures of 650ºC (roughly 1,200ºF) and above, non-precious metals can be used as catalysts at the anode and cathode, reducing costs. Unlike alkaline, phosphoric acid, and polymer electrolyte membrane fuel cells, MCFCs don't require an external reformer to convert more energy-dense fuels to hydrogen. Due to the high temperatures at which they operate, these fuels are converted to hydrogen within the fuel cell itself by a process called internal reforming, which also reduces cost.

DMFC is similar to the PEMFC in that the electrolyte is a polymer and the charge carrier is the hydrogen ion (proton). However, the liquid methanol (CH_3OH) is oxidized in the presence of water at the anode generating CO_2, hydrogen ions and the electrons that travel through the external circuit as the electric output of the fuel cell. The hydrogen ions travel through the electrolyte and react with oxygen from the air and the electrons from the external circuit to form water at the anode completing the circuit. Current DMFCs are limited in the power they can produce, but can still store high energy content in a small space. This means they can produce a small amount of power over a long period of time [2]. This makes them presently ill-suited for powering vehicles, but ideal for consumer goods such as mobile phones, digital cameras or laptops.

Solid oxide fuel cells operate at very high temperatures—around 1,000ºC. High temperature operation removes the need for precious-metal catalyst, thereby reducing cost [1]. It also allows SOFCs to reform fuels internally, which enables the use of a variety of fuels and reduces the cost associated with adding a reformer to the system. High-temperature operation has disadvantages. It results in a slow start up and requires significant thermal shielding to retain heat and protect personnel, which may be acceptable for utility applications but not for transportation and small portable applications. The high operating temperatures also place stringent durability requirements on materials [2].

1.5 Why Solid Oxide Fuel Cell (SOFC)

Solid oxide fuel cells (SOFCs) are energy conversion devices that produce electricity and heat directly from a gaseous or gasified fuel by electrochemical combination of that fuel with an oxidant. A SOFC consists of an interconnect structure and a three-layer region composed of two ceramic electrodes, anode and cathode, separated by a dense ceramic electrolyte (often referred to as the PEN—Positive-electrode/ Electrolyte/Negative-electrode). SOFCs operate at high temperatures and atmospheric or elevated pressures, and can use hydrogen, carbon monoxide, and hydrocarbons as fuel, and air (or oxygen) as oxidant. In the cell, the oxygen ions formed at the cathode migrate through the ion-conducting electrolyte to the anode/electrolyte interface where they react with the hydrogen and carbon monoxide contained in (and/or produced by) the fuel, producing water and carbon dioxide while releasing electrons that flow via an external circuit to the cathode/electrolyte interface. Solid oxide fuel cells are

the most efficient among all the types of fuel cells we have. The reasons for choosing SOFC for my present thesis include its fuel flexibility, internal reforming, efficiency, cogeneration possibility, simple design and its environmental impact.

SOFCs employ a thin ceramic membrane as an electrolyte. Oxygen ions (O^{2-}) are the ionic charge carrier in an SOFC membrane. The most common SOFC electrolyte is an oxide material called yttria-stabilized zirconia (YSZ). In a H_2-O_2 SOFC, the electrochemical half reactions are

$$H_2 + O^{2-} \rightarrow H_2O + 2e^- \text{ (Anode)}$$

$$\frac{1}{2}O_2 + 2e^- \rightarrow O^{2-} \text{ (Cathode)}$$

$$H_2 + \frac{1}{2}O_2 \rightarrow H_2O \text{ (Net reaction)}$$

To function properly, SOFC's must operate at high temperatures (> 600^{o}C). They are attractive for stationary applications because they are highly efficient and fuel flexible.

SOFC can use any type of fuel for the production of electricity as it operates at very high temperatures around 1000^{o}C. At these high working temperatures internal reforming of the hydrocarbons takes place within the system and this can reduce the high cost external reforming techniques and allows us to use any kind to fuel for its operation. For combined heat and power (CHP) applications the efficiency of the fuel cell may reach as high as 80% and this also allows possibility of cogeneration, where the high temperature from the SOFC is used to run a turbine. As all the parts of SOFC are in solid state with ceramic materials it has the simplest design with high stability which allows easy manufacturing techniques. This type of fuel cell is the cleanest with low noise and low emissions.

1.6 History and Literature Review

Solid oxide fuel cells (SOFCs) are the most efficient devices yet invented for conversion of chemical fuels directly into electrical power. Originally the basic idea and materials were proposed by Nernst and his colleagues in Gottingen at the end of the nineteenth century, but considerable advances in theory and experiment are still made over 100 years later.

The principle of fuel cell operation were first reported by Sir William Grove in 1839, ceramic came much later and began with Nernst's discovery of solid oxide electrolyte in 1899 and the operation of the first ceramic fuel cell at 1000^{o}C by Baur and Preis in 1937.

The science and technology of ceramic fuel cells and the critical issues posed by the development of this type of fuel cell were discussed by Nguyen and Minh [5]. Use of solid electrolyte in ceramic fuel cells eliminates material corrosion and electrolyte management problems. All the components of solid-oxide (ceramic) fuel cell should have similar thermal expansion coefficients. They also discussed about the types of designs, flow patterns and the manufacturing technologies.

Yamamoto et al. [6] reviewed the science and technologies of solid oxide fuel cells with emphasis on discussion of their component materials. Except for cost-effective manufacturing processes, the development efforts over the past 30 years have brought the technology of high temperature SOFC near its final goal. On the other hand, technology of intermediate temperature SOFCs is still in a developmental stage and several technological challenges remain to be solved before this type of fuel cell can find practical applications.

Barnett et al. [7] used solid oxide fuel cells (SOFCs) with thin yttria-stabilized zirconia (YSZ) electrolytes on porous Ni-YSZ anodes which were successfully operated with humidified methane and natural gas. Conventional anode supported SOFCs can be operated directly with humidified methane and natural gas, yielding high open circuit voltages and high power densities. Very little carbon was detected on the anodes, suggesting that carbon deposition was limited during cell operation.

Porous composite solid oxide fuel cell (SOFC) electrodes formed by a mixture of electronic conductor and ionic conductor particles of small size have been studied by Costamagna et al. [8] by means of an analytical simulation model. Morphological effects show strong influence on the electrode resistance i.e; too thin an electrode, then too small the active area for the electrochemical reactions; too thick an electrode, then too high the ohmic losses.

A three-dimensional mathematical model for a planar SOFC was constructed by Yakabe et al. [9] to calculate concentration of the chemical species, the temperature distribution, the potential distribution and the current density using a single-unit model with double channels of co-flow or counter-flow patterns. The internal or external steam-reforming, the water-shift reaction and the diffusion of gases in the porous electrodes were taken into the model. They also investigated the effect of the cell size, the operating voltage and the thermal conductivity of the cell components. From the simulated temperature distributions in the electrolyte and the inter-connector, the stress distributions were calculated using the finite element method. The results demonstrated that steam reforming would generate high internal stress in an electrolyte.

Internal steam reforming in SOFC leads to inhomogeneous temperature distributions according to the fast reforming reaction kinetics. This results in thermal induced stresses and may lead therefore to mechanical failure of the material. A one-dimensional numerical simulation program has been developed by Thom et al. [10] to describe the transport of gases inside the SOFC anode due to diffusion and permeation as well as the kinetic of the reforming reaction and the electrochemistry.

Reforming of hydrocarbon fuels for SOFCs can be done without additional gas purification. As both stack and hydrocarbon reformer unit have to be operated at high temperatures (700–1000°C), thermal management plays an important role in the successful operation of SOFC systems this may be achieved by suitable selection of materials and right system of design and control strategies. For this Apfel et al. [11] built a finite element simulation for complete SOFC systems which allows studying system parameters both during steady operation and during transients.

Lin et al. [12] in their short communication describes the effect of interconnect rib size on the fuel cell concentration polarization in planar SOFCs as a function of the different physical and geometrical parameters formulating the model in a dimensionless framework, enabling a generalization of the results in terms of one characteristic diffusion parameter and one dimensionless geometry parameter. Based on the results from their analytical solution for smaller rib width compared to the penetration distance of the reactant species, the gas concentration is uniform and concentration polarization with the rib presence takes the same form as that without ribs except that the effective current density should be used. When the rib size is comparably large then it has high concentration polarization.

Grondin et al. [13] developed a three-dimensional model to investigate the effect of interconnect design on the electrical performance and degradation process. As cathode degradation is supposed due to temperature gradient non-uniformity they demonstrated the impact of cathode/interconnect contact on thermal and electrical behavior. In this investigation, the effects of the two geometrical parameters are considered, the modification of cathode/interconnect contact area and electrical collecting pins size. From their simulations decreasing power density and a reduction of temperature gradient for an increasing contact area are seen and decreasing size of collecting pins, better temperature homogeneity and power density are recorded.

Complete polarization model of a solid oxide fuel cell (SOFC) that eliminates the ambiguity of the suitability of such model when used under different design and operating conditions were discussed by Chan et al. [14]. The Butler-Volmer equation is used in the model to describe the activation overpotential. In the concentration overpotential, both ordinary and Knudsen diffusions are considered to cater for different porous electrode designs. Results show that the performance of an anode-supported fuel cell is superior to that using cathode as the support under elevated operating pressures.

A one-dimensional numerical simulation program has been developed by Lehnert et al. [15] to describe the transport of gases inside the SOFC anode due to diffusion and permeation as well as the kinetic of the reforming reaction and the electrochemistry. They performed the sensitivity analysis to reduce the methane conversion rate. Internal steam reforming in SOFC cells leads to inhomogeneous temperature distributions according to the fast reforming reaction kinetics. This results in thermal induced stresses and may lead therefore to mechanical failure of the material.

A quasi-two- (co- and counter-flow) and three- (cross-flow) dimensional simulation program for planar-type SOFC was made by Iwata et al. [16] considering mass, charge and heat balances along the flow directions and perpendicular to the electrolyte membrane, in order to obtain temperature and current density distributions along the flow direction. Numerical results from this simulation with adiabatic boundary conditions show that the temperature increases along the flow direction in the co-flow case and the temperature profile has a maximum near the fuel inlet in the counter-flow case.

A new numerical model which enables to calculate the electric current path inside the cell components was presented by Yakabe and Sakurai [17]. This new model analyses made it possible to simulate the diagonal electric current in the electrolyte, and, in addition, the effects of the geometry of the cell components on the cell performance was considered perfectly in the calculation. It was made clear that if there is a large distribution of the electromotive force in the single-cell, the diagonal flow of the electric current appears in the electrolyte.

The solid oxide fuel cell (SOFC) has a problem in durability of the ceramics used as its cell materials because its operating temperature is very high and the cell temperature fluctuation induces thermal stress in the ceramics. The cell temperature distribution in the SOFC, therefore, should be kept as constant as possible during variable load operation through control of the average current density in the cell. Considering this fact, Inui et al. [18] numerically optimized the operating parameters of air utilization and the inlet gas temperature of the planar SOFC by minimizing the cell temperature shift

from its nominal value and propose a new cell temperature control method that adopts these optimum operating parameters for each average current density.

The three-dimensional simulation code of the planar SOFC stack and the detailed effect of radiation heat transfer is investigated by Tanaka et al. [19]. The whole stack simulation is needed to calculate accurately the cell voltage because the radiation heat transfer reduces it when the ambient temperature is low. The bad influence of the low ambient temperature on the voltage is, however, small and a relatively high voltage are obtained even when the ambient temperature is very low.

Janardhanan et al. [20] performed analysis on the planar solid oxide fuel cell under direct internal reforming condition; they found significant differences in efficiency and power densities for isothermal and adiabatic operational regimes. For pre-reformed fuel case, adiabatic operation results in lower performance compared to isothermal operation. It is further discussed that, though direct internal reforming may lead to cost reduction and increased efficiency by effective utilization of waste heat, the efficiency of the fuel cell itself is higher for pre-reformed fuel compared to non-reformed fuel.

A numerical simulation tool for calculating the planar solid oxide fuel cells was described by Wang et al. [21], where they employed finite volume method for the simulation (ANSYS-CFX®). Simulation results show that the co-flow case has more uniform temperature and current density distributions and smaller temperature gradients, thus offers thermal structural advantages than the counter-flow case, further it is effective to improve the output voltage by reducing the thickness of anode or increasing its porosity.

Transient thermal analysis plays a central role in the design and optimization of high temperature solid oxide fuel cells (SOFCs) during startup/shutdown, because of the potential for damaging thermal gradients to develop within the SOFC components. Here Damm and Fedorov [22] consider the SOFC unit cell, which is heated by hot air supplied into the oxidizer channel at a specified, time-dependent inlet temperature and develop and evaluate limiting cases that allow closed-form analytical solutions of the time-varying temperature fields, from which heating time and maximum temperature gradient are calculated. Results indicate that the reduced-order models' simplicity, computational savings, and ability to capture the essential physics of the transient process justify their use in design calculations over more complex, highly detailed, numerical/CFD schemes.

Ho et al. [23] presented a numerical model for a planar SOFC with mixed ionic-electronic conducting electrodes. The coupled equations describing the conservation of mass, momentum and energy and the chemical and electrochemical processes are solved.

1.7 Motivation for the Thesis

The fuel cells are one of the promising technologies, attracting the global market in the field of renewable energy sources. Enhancing the fuel cell efficiency and reducing its cost are two key objectives in the research and development of fuel cell technologies. It is very difficult to understand the heat and mass transfer coupled with electrochemical reactions in fuel cell. It is crucially important to understand the physics inside the fuel cell in order to improve its performance. While the experiments are expensive to implement and subject to practical limitations, cost effective numerical modeling and simulation can provide such information and predict effects of different factors including

interconnect design, channel length and various parameters which leads to better design with optimized performance.

Many numerical models have been developed to predict the cell performance. Some of them focus on the materials for different parts of the fuel cell, some focus on the high temperature performances for stress analysis, while some focus on the internal reforming of the hydrocarbons. However, there are few research publications on the overall SOFC modeling, in particular, coupled with the interconnect design, heat and mass transfer and electrochemical reactions. This motivates the thesis author to develop a numerical model for the entire SOFC and optimize the cell performance by the various interconnect contact surface areas and operating parameters. The developed model will give a clear view of the SOFCs, and help engineers to understand the effects of those parameters, which can significantly improve the cell performance.

1.8 Research Objectives

These days SOFCs receive serious attention and many researchers are trying to improve its efficiency and working to reduce the operating temperature. Thermal management, improved fluid flow, proper interconnect and channel design are the promising path ways. High temperature causes thermal stresses which leads to the degradation of the materials thereby causing improper working of the fuel cell. In this thesis, four research objectives were pursued, which are listed below:

- To create a single channel fuel cell model, including flow channels, interconnects, electrodes and electrolyte.

- Simulate the hydrodynamic, heat transfer and electrochemical phenomena to obtain the fuel cell performance information.
- Simulating the hydrodynamic, heat transfer and electrochemical phenomena for fuel cell with different interconnect designs to obtain the temperature and polarization curves.
- Optimize the SOFC interconnect design depending on the results obtained from the above task and perform the parametric study.

1.9 Thesis Outline

In this thesis, the three-dimensional CFD model has been developed to optimize the interconnect design for SOFC and a parametric study is performed. Chapter 2 will discuss the SOFC modeling including the fundamentals of the electrochemistry and fuel cells. This model is validated using a three-dimensional single channel SOFC case. Chapter 3 discusses the numerical modeling for different interconnect designs of the single unit SOFC. Temperature distribution, electrical performance and mass fraction of the species are investigated. Chapter 4 focuses on the optimized design case and a parametric study is carried with different mass flows, hydraulic diameters and interconnects material properties. Chapter 5 concludes the current research, and some recommended future work is summarized.

CHAPTER 2

SOFC MODEL AND VALIDATION

2.1 SOFC Model

A three-dimensional SOFC single cell is shown in Fig. 2.1 which includes interconnects, anode/cathode gas channels, gas diffusion electrodes (GDEs) and electrolyte totally to divide into seven zones. A one-dimensional schematic drawing is also shown in Fig. 2.2 to have clear view of the fuel cell working. The hydrogen gas mixture flows through the anode gas channel. Then it diffuses into the porous ceramic anode electrode and contacts with the active surface on the electrolyte known as TPB (Triple Phase Boundary). TPB is the surface where all the three important phases - electrolyte, gas and electrically connected catalyst regions are in contact. On the cathode side, the oxygen mixture flows through the cathode gas channel and diffuses through the porous cathode electrode. After that, oxygen contacts the active surface on the electrolyte at the cathode side and produces oxygen ions which are the ionic charge carriers in an SOFC electrolyte membrane. These oxygen ions migrate through the electrolyte membrane to come in contact with hydrogen on the other side to form water. The anode half reaction is an oxidation reaction; the electrons produced travel along the external circuit and reach the cathode for oxygen reduction reaction there by completing an electrical circuit. As the operating temperature of the SOFCs is above 600^{o}C all the species are in gaseous state. The chemical reactions can be expressed as:

At anode: $$H_2(g) + O^{2-} \leftrightarrow H_2O(g) + 2e^- \text{ (oxidation)} \quad (2\text{-}1)$$

At cathode: $$\frac{1}{2}O_2(g) + 2e^- \leftrightarrow O^{2-} \text{ (reduction)} \quad (2\text{-}2)$$

Overall: $$H_2(g) + \frac{1}{2}O_2(g) \leftrightarrow H_2O(g) \quad (2\text{-}3)$$

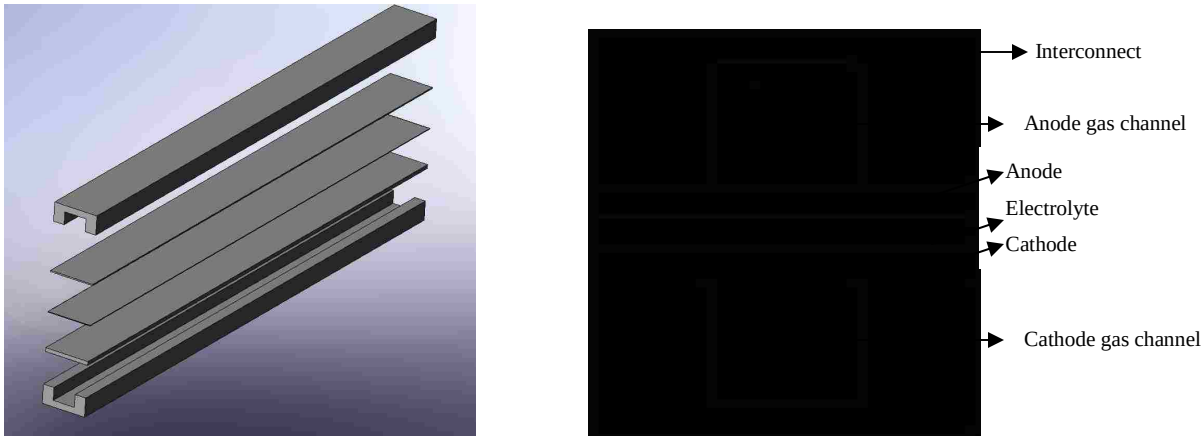

(a) (b)

Fig. 2.1 (a) Three-dimensional solid works model of SOFC
(b) Two-dimensional front view

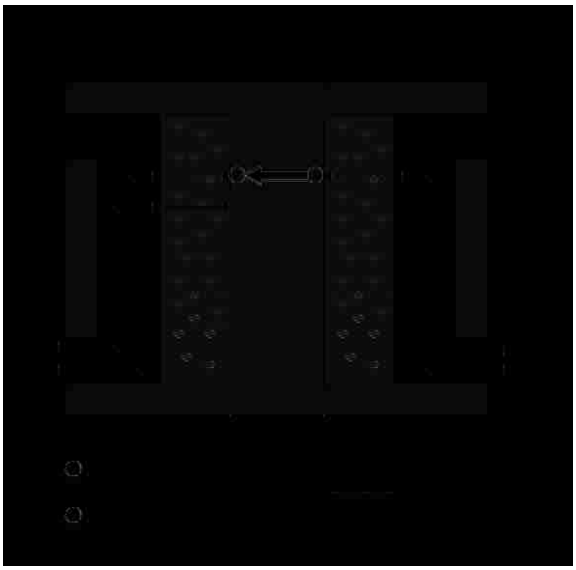

Fig. 2.2 Schematic one-dimensional SOFC model

In order to model SOFCs, it is necessary to understand the mass, momentum and energy transport, electrochemical reactions and charge balance inside the fuel cell.

However, it is very difficult to take every single detail of the whole process into account which includes tremendous computational time. Some basic assumptions are necessary to simplify the SOFC model, including:

- Steady-state operation
- Ideal gas mixtures
- Single-phase flow
- Isotropic electrodes and electrolyte
- Incompressible flow
- Neglect contact resistance of current collector and electrodes

We can use the concept of flux balance to solve for the one-dimensional SOFC model making number of assumptions. However, these numerous assumptions lessen the accuracy of the model for design purpose. So, we rely on the full three-dimensional analysis of the fuel cell using sophisticated numerical modeling techniques. Computational fluid dynamics (CFD) allows us to estimate more accurate results of fuel cell performance. More importantly, CFD can provide three-dimensional localized information inside the fuel cell. The governing equations employed by CFD models start with the conservation laws. These governing equations are modified according to the specific problem.

2.1.1 Mass Conservation

The mass conservation equation (or continuity equation) simply requires that the rate of mass change in a unit volume must be equal to the sum of all the species entering (exiting) the volume in a given time period.

$$\frac{\partial}{\partial t}(\varepsilon\rho) + \nabla \bullet (\varepsilon\rho U) = 0 \tag{2-4}$$

The above equation is modified and expressed as:

$$\nabla \bullet (\rho U) = S_{mass} \tag{2-5}$$

where ρ is the density (kg/m^3), U is the velocity (m/s), ε is porosity implemented in this equation to account for porous domains such as electrode and gas channels and S_{mass} is the source term. In the mass conservation equation it has different source terms in different cell zones. At the electrode/electrolyte interface, there are hydrogen/oxygen consumption and water formation. The mass sink and source rate depend on the electrochemical reaction rates. Thus they can be calculated by:

$$S_{H_2} = -\frac{M_{w,H_2}}{2F} i_{an} \tag{2-6}$$

$$S_{O_2} = -\frac{M_{w,O_2}}{4F} i_{cat} \tag{2-7}$$

$$S_{H_2O} = \frac{M_{w,H_2O}}{2F} i_{cat} \tag{2-8}$$

where M_w is the molecular weight, i is the current density and F is the Faraday constant (96500C/mol).

2.1.2 Momentum Conservation

Similarly to the mass conservation equation, we can set up an equation using vector form for momentum conservation as:

$$\frac{\partial}{\partial t}(\varepsilon\rho U) + \nabla \bullet (\varepsilon\rho UU) = -\varepsilon\nabla p + \nabla \bullet (\varepsilon\zeta) + \frac{\varepsilon^2 \mu U}{\kappa} \tag{2-9}$$

where ζ and μ stand for the shear stress tensor and the fluid dynamic viscosity, respectively. The weakly compressible Navier-Stokes equations govern the flow in the open channels:

$$\rho(u \bullet \nabla)u = \nabla \bullet \left[-pI + \frac{\mu}{\varepsilon}\left(\nabla u + (\nabla u)^T\right) - \frac{2}{3}(\nabla \bullet u)I \right] \tag{2-10}$$

$$\nabla \bullet (\rho u) = 0 \tag{2-11}$$

In the porous GDEs, the Brinkman equation describes the flow velocity:

$$\left(\frac{\mu}{\kappa} + Q\right)u = \nabla \bullet \left[-pI + \frac{\mu}{\varepsilon}\left(\nabla u + (\nabla u)^T\right) - \frac{2}{3}(\nabla \bullet u)I \right] \tag{2-12}$$

$$\nabla \bullet (\rho u) = Q \tag{2-13}$$

where ε and κ denotes, respectively, the porosity and permeability (m^2) of the medium, I is the identity matrix and Q is the mass source term, which relates to the charge transfer current density i_{ct} according to:

$$Q = \sum_i S_a \frac{i_{ct,i} M_i}{n_i F} \tag{2-14}$$

where S_a is the specific surface area and n stands for the number of moles of electrons transferred. Solving the momentum conservation equation permits us to obtain the pressure (p) distribution of the fluids flowing through the fuel cell.

2.1.3 Species Conservation

The mass conservation and the momentum conservation equations discussed above are used to describe the over all bulk motion of the fluid mixture. In contrast, the species conservation equation describes the differential movement of each individual species within the fluid mixture.

$$\frac{\partial}{\partial t}\left(\varepsilon\rho \mathrm{X}_i\right)+\nabla \bullet\left(\varepsilon\rho U x_i\right)=\nabla \bullet\left(\rho D_i^{eff} \nabla x_i\right)+\dot{S}_i \tag{2-15}$$

where x_i and D_i^{eff} stands for species mass fraction and effective diffusivity (m^2/s) of each species i. The material transport is described by the Maxwell-Stefan's diffusion and convection equation. Let ω_i be the weight fraction of species i. In the stationary case, the mass balance is governed by:

$$\nabla \bullet\left(\omega_i \rho u-\rho \omega_i \sum_{j=1}^{k} \tilde{\tilde{D}}_{ij}\left(\frac{M}{M_j}\left(\nabla \omega_j+\omega_j \frac{\nabla M}{M}\right)+\left(x_j-\omega_j\right)\frac{\nabla p}{p}\right)\right)=R_i \tag{2-16}$$

where $\tilde{\tilde{D}}_{ij}$ represents the ij components of the multi-component Fick diffusivity, which is calculated from the Maxwell-Stefan diffusivity, D_{ij} (m^2/s) as,

Fick diffusivity: $$J_i=-c_t \tilde{\tilde{D}}_{ij} \nabla x_i \tag{2-17}$$

Maxwell-Stefan diffusivity: $$\nabla x_i=\frac{-x_i x_j\left(u_i-u_j\right)}{D_{ij}} \tag{2-18}$$

where J_i is the diffusion flux (mol/m^2-s), c_t is the total mixture molar concentration (mol/m^3), u is the velocity (m/s), ρ is the density of the fluid (kg/m^3), p the pressure (Pa), and R_i is the reaction source term for species i (kg/m^3-s), and x_j the molar fraction of species j. The average molecular weight is calculated as:

$$M=\sum_{j=1}^{k} x_j M_j \tag{2-19}$$

where M_j is the molar mass of species j (kg/mol). Assume the gas to be ideal, so that the density is given by

$$\rho = \frac{pM}{RT} \tag{2-20}$$

In the open channel, the reaction source term is set to zero. However, in the GDEs, the source term is given by the electrochemical reaction rate. It is calculated from the charge transfer current density according to the Faraday's law

$$R_i = \nu_i \frac{i_{ct,i} M_i}{n_i F} \tag{2-21}$$

where ν_i is the stoichiometric coefficient and n_i is the number of electrons in the reaction.

2.1.4 Energy conservation

The energy conservation equation describes the thermal balance within the fuel cell.

$$\frac{\partial}{\partial t}(\varepsilon \rho h) + \nabla \bullet (\varepsilon \rho U h) = \nabla \bullet k^{eff} \nabla T + \varepsilon \frac{dp}{dt} - j\eta + \frac{\hat{i} \bullet \hat{i}}{\sigma} + S_T \tag{2-22}$$

where h and k^{eff} stand for enthalpy of the fluid flowing through the fuel cell and its effective thermal conductivity respectively. The fluid enthalpy may be calculated based on the species present in the fluid and the fluid temperature, T. The first term on the RHS accounts for the rate of energy change due to thermal conduction. The second term on the RHS accounts for rate of energy change due to the mechanical work of the fluids. In the last three terms on the RHS, η, $\hat{i}$, σ, S_T stand for overvoltage, current flux vector, electric conductivity and heat sources, respectively.

During the electrochemical reaction, the heat source includes the ohmic heat and reaction heat. In different zones, the heat source is different, such as in GDEs, the

reaction heat is the primary part; while in electrolyte, ohmic heat is the main heat source. From our basic assumptions the above general equation is simplified as:

$$\nabla \bullet \left(\rho_i U_i T\right) = \nabla \bullet \left(k^{eff} \nabla T\right) + S_T \tag{2-23}$$

where source term $S_T = I^2 R_{ohm} + h + \eta_{an} i_{an} + \eta_{cat} i_{cat}$, k^{eff} is the effective thermal conductivity (W/m-K), I is the electric current (A), R is the electric resistance (ohm).

2.1.5 Charge Conservation

From the continuity of current in a conducting material,

$$\nabla \bullet \hat{i} = 0 \tag{2-24}$$

where i stands for the current flux vector. Two types of charges are present in fuel cell systems-electrons and ions. Since, both types of charge are generated from originally neutral species (hydrogen and/or oxygen), overall charge neutrality must be conserved.

$$\nabla \bullet i_{elec} + \nabla \bullet i_{ion} = 0 \tag{2-25}$$

where i_{ion} stands for the ionic current through an ion conducting phase such as the catalyst layer or membrane and i_{elec} stands for the electronic current in an electron conducting phase such as a catalyst layer or electrode. The electronic charge balance in the anode current feeders is given by:

$$\nabla \bullet \left(-\sigma_1 \nabla \phi_{elec}\right) = 0 \tag{2-26}$$

where σ_1 denotes the electronic conductivity of the current feeder and ϕ_{elec} is its electronic potential. Similarly, the ionic charge balance, valid in the ionic conductor is:

$$\nabla \bullet \left(-\sigma_2 \nabla \phi_{ion}\right) = 0 \tag{2-27}$$

where σ_2 is the ionic conductivity and ϕ_{ion} is the ionic potential.

In the anode and cathode GDE, electrons are transferred between the ionic conducting electrolyte phase and the electronically conducting phase. This implies that the charge balance equation have current source terms present as:

$$\nabla \bullet \left(-\sigma_1 \nabla \phi_{elec}\right) = S_a i_{ict} \tag{2-28}$$

$$\nabla \bullet \left(-\sigma_2 \nabla \phi_{ion}\right) = S_a i_{ict} \tag{2-29}$$

where $S_a i_{ict}$ denotes the specific surface area S_a times the charge transfer current reaction density i_{ict}. To solve these above two equations, the boundary conditions are specified. Electrons pass through the anode and cathode current collector to the external electric circuit. At the anode side, the electrode voltage is usually set as 0V, while at the cathode side; the electrode voltage is set as the cell voltage. For the electric field, the boundary conditions are:

$$\phi_{elec} = 0 \qquad \text{(anode)} \tag{2-30}$$

$$\phi_{elec} = V_{cell} \qquad \text{(cathode)} \tag{2-31}$$

For the ionic field, there are no ions transferring through any current collector. The boundary conditions are:

$$\frac{\partial \phi_{electrolyte}}{\partial \hat{n}} = 0 \tag{2-32}$$

where $\hat{n}$ is the unit vector, pointing outward on the boundaries.

Assume that Butler-Volmer charge transfer kinetics describe the charge transfer current density. At the anode, hydrogen is reduced to form water, and the following charge transfer kinetics equation thus applies:

$$i_{a.ct} = i_{0,a} x_{H_2} \frac{c_t}{c_{H_2.ref}} \left[\exp\left(\frac{\alpha F \eta}{RT}\right) - \exp\left(\frac{-(1-\alpha) F \eta}{RT}\right) \right] \tag{2-33}$$

where $i_{0,a}$ is the anode exchange current density (A/m^2), x_{H_2} is the molar fraction of hydrogen, c_t the total concentration of the species (mol/m^3), and $c_{H_2,ref}$ is the reference concentration (mol/m^3). Furthermore, F is the Faraday's constant (96500 C/mol), R is the gas constant (J/ mol-K), T is the temperature (K) and η is the overvoltage (V).

For the cathode, the relation is:

$$i_{c.ct} = i_{0,c} x_{O_2} \frac{c_t}{c_{O_2.ref}} \left[\exp\left(\frac{\alpha F \eta}{RT} \right) - \exp\left(\frac{-(1-\alpha) F \eta}{RT} \right) \right] \tag{2-34}$$

where $i_{0,c}$ is the cathode exchange current density (A/m^2), and x_{O_2} is the molar fraction of oxygen.

During the chemical reaction, the driving force is the overpotential between the solid electronic phase ϕ_{elec} and the ionic phase ϕ_{ion}, which is also known as the activation loss η. The overpotential is defined as:

$$\eta = \phi_{elec} - \phi_{ion} - \Delta\phi_{eq} \tag{2-35}$$

where $\Delta\phi_{eq}$ is the equilibrium potential difference (V).

At the cathode side the cell voltage V_{cell} is defined as:

$$V_{cell} = \Delta\phi_{eq,c} - \Delta\phi_{eq,a} - V_{pol} \tag{2-36}$$

where V_{pol} is the polarization. In our simulations, $\Delta\phi_{eq,a}$ = 0V and $\Delta\phi_{eq,c}$ = 1V and we change V_{pol} as the parameter. For ionic charge balance equations, applying perfect insulating boundary conditions at all external boundaries and for the interior boundaries, continuity in current and potential applies by default.

2.2 Numerical Method

A finite volume method has been applied to simulate thermal behavior of SOFC. The computational mesh has been created using commercial software Gambit® and it is loaded into the CFD software Fluent® to calculate temperature profiles. A part of the computational domain is considered and simulations were performed to investigate the electrical performance of the fuel cell using the commercial software COMSOL® multiphysics which uses finite element method. Due to the memory constraint in COMSOL® the entire fuel cell simulation is difficult to perform. The computational mesh for simulating electrical behavior has been created using COMSOL® itself.

2.2.1 Computational Domain

In order to validate the developed SOFC numerical model, a single channel, three-dimensional numerical model has been created with seven zones, which are anode/cathode current collectors, anode/cathode gas channels, anode/cathode gas diffusion electrodes and electrolyte membrane (see in Fig. 2.1). The model dimensions are listed in Figure 2.3 and Table 2.1, which are chosen based on the work by Yakabe et al. [9], who have conducted a parametric study of single channel SOFC performance. The current collector contacts with the gas diffusion layer while the gas mixtures flow through the inner channels surrounded by the current collector. The electrodes/electrolyte assembly locates at the center of SOFC with three layers.

Table 2.1 Dimensions of single channel SOFC model

Dimensions	Value
Gas channel length	100 mm
Gas channel width	2 mm
Gas channel height	1 mm
Electrolyte layer thickness	0.1 mm
Anode layer thickness	0.15 mm
Cathode layer thickness	0.1 mm
Current collector width	4 mm
Current collector height	2 mm

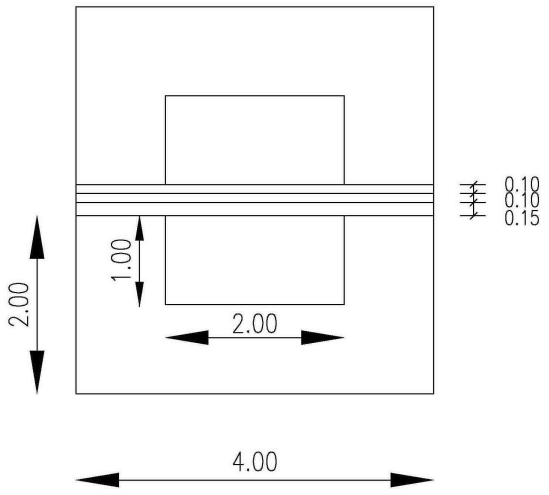

Fig 2.3 Front view of a single channel SOFC (units: mm)

From Fig 2.3, the membrane electrode assembly, including the anode/cathode electrode layers and the electrolyte, has a sandwich structure. The current collector contacts with the GDE's outer surfaces. Based on the assumption of the periodic

conditions between each channels, it is reasonable to simulate only a single channel computational domain. In the real fuel cell active areas, there are thirty or more channels. Those channels are relatively long, compared to the channels' width and height. Usually the transport phenomena are similar between those channels. Another reason is the computational power limitation of current research techniques. SOFC model contains many transport equations and each of them is coupled with another, such as the energy equation coupled with the hydrodynamics equations, the species transport equation coupled with the electrochemical equation, etc. Many properties have been approximated based on velocity, temperature, pressure and other variables. Those require a huge amount of computing tasks. So that this single channel SOFC model is reasonable and affordable. After the model validation for the single channel solid oxide fuel cell, it will be very straightforward to apply it to SOFCs with other geometries and design cases.

Fig 2.4 shows the part of the computational mesh with 188,000 cells and 217,974 nodes, which is created using the Gambit® software. It includes the aforementioned seven zones. The hexahedral type mesh is applied, because the computational domain is rectangular. The heat transfer simulations are performed using Fluent® software and only the middle some part of the above mentioned computational mesh is taken and the electrochemical simulations are performed using a general purpose multi-physics package, COMSOL® (FEMLAB) software.

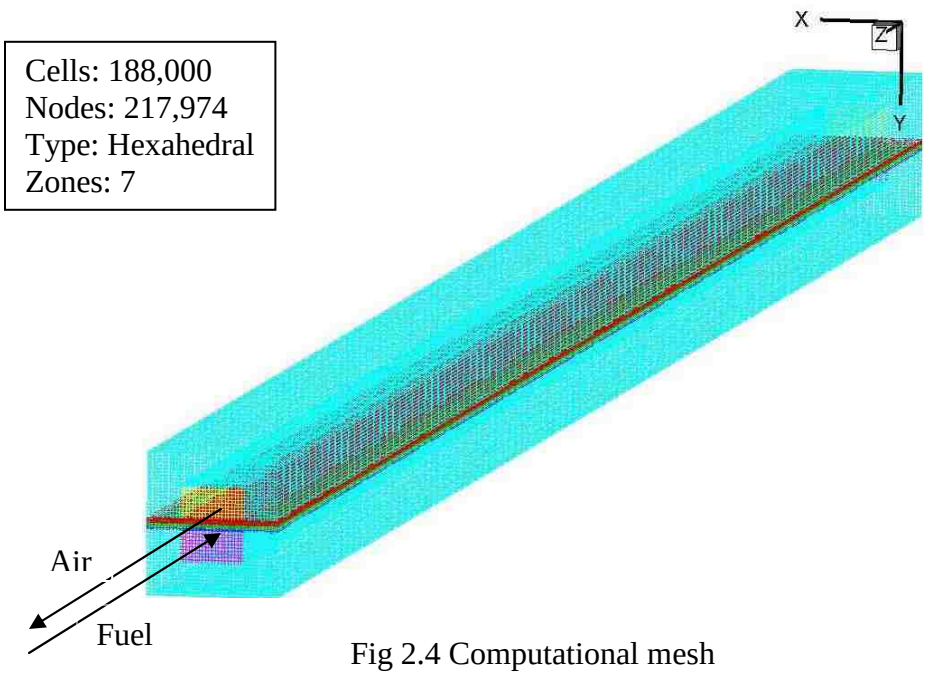

Fig 2.4 Computational mesh

2.2.2 Boundary Conditions

1) Mass Inlet

In this single channel SOFC model, there are two inlets: hydrogen mixture inlet (anode), air inlet (cathode). The velocity inlet condition is used for both the inlets which are counter flow type. According to work done by Yakabe et al. [9] air velocity is taken as 3 m/s and fuel velocity as 0.4 m/s and applied in the momentum equation.

The material transport is described by the Maxwell-Stefan's diffusion and convection equation which is described above. The inlet fluid in the SOFC is the gas mixture. At the anode side, the gas components are hydrogen and water vapor, while in the cathode side, it contains the oxygen, water vapor and nitrogen. The mass fraction is set as 0.4 for hydrogen and 0.6 for water vapor in anode fuel mixture. In the cathode the air mass fraction is set as 0.15 for oxygen and 0.37 for water vapor and the rest for nitrogen. The diffusivity D_{ij} for the species is calculated using the kinetic volumes from the equation.

$$D_{ij} = k_d \left[\frac{T^{1.75}}{p_{atm}\left(v_i^{1/3} + v_j^{1/3}\right)^2 \left[\frac{1}{M_i} + \frac{1}{M_j}\right]^{0.5}} \right] \tag{2-37}$$

$$D_{ij}^{eff} = D_{ij}\varepsilon^{1.5} \tag{2-38}$$

where k_d is the reference diffusivity, v is the kinetic volume of the species, D_{ij}^{eff} is the effective diffusivity, T is the temperature (K) and ε stands for porosity of the flow structure.

2) Thermal Boundary Conditions

The energy equation is solved to obtain the temperature distribution within the solid oxide fuel cell. Heat is generated by the electrochemical reaction in the electrolyte/electrode contact layers and the current flow in the inter-connector. The "coupled" heat transfer is solved between the fluid zones (fluid in gas channels) and the solid zone (the current collectors, the electrolyte and the electrodes). The inlet fuel temperature is set as 1073K and the air temperature as 873K, which is the operating condition used by Yakabe et al. [9]. The side walls of the fuel cell are considered as adiabatic since it is assumed as the periodic conditions of parallel channels.

3) Fluid Flow

The gas mixture is assumed to be an incompressible fluid. At the wall boundary, a non-slip boundary condition is assumed. The inlet mass flow rate of the gas mixture is set according to Equations (2-12) and (2-13). The outlet boundary condition is the pressure outlet with no viscous stress and the outlet pressure is set to the atmospheric pressure.

4) Fluid and Solid Zones

The gas channels and the electrode structures are the different types of fluid zone, while the others are of solid zones. The electrode structures are also porous zones, the gas channels are the normal fluid zone. In the current collector zones, for the energy equation, the source term is the ohmic heat source. For the interface layers, they are fluid zones and the gas mixture will diffuse through them. The electrode layers have three source terms for different equations: electric potential field Equation (2-26), protonic potential field Equation (2-27) and mass conservation Equation (2-5). In the electrode layers, the source term of the energy equation needs the additional term, which accounts for the chemical reaction heat generation at the electrode/electrolyte interface. The catalyst is the solid zone. The ohmic heat generation is used in the energy equation.

2.2.3 SOFC Model

The SOFC model is now brought into the COMSOL® software with SOFC module loaded into it. There are many parameters to be set properly and many scalar equations which need to be defined prior to starting the simulations. In the published literature, different research groups have used different sets of parameters based on the materials, temperatures and the fuel cell operating conditions. In order to validate the SOFC model, the parameters are carefully set according to the physical properties in the research work done by Yakabe et al. [9], the total SOFC parameters are listed in Table 2.2, which include the electrochemical reaction, species transport and heat transfer parameters. Some of the missing parameters are taken from other research groups Achenbach et al. [25].

Table 2.2 SOFC parameters [9]

Parameters	Value
Anode exchange current	1 [A/ m^2]
Anode specific surface area	10e8 [1/m]
Anode permeability	1e-13 [m^2]
Anode equilibrium voltage	0 [V]
Anode thermal conductivity	1.86 [W/m-K]
Cathode exchange current	0.1 [A/m^2]
Cathode specific surface area	10e8 [1/m]
Cathode permeability	1e-13 [m^2]
Cathode equilibrium voltage	1 [V]
Cathode thermal conductivity	5.84 [W/m-K]
Viscosity of air	3e-5 [kg/(m-s)]
Initial cell polarization	0.05 [V]
Electrolyte effective conductivity, anode	1 [S/m]
Solid effective conductivity, anode	1000 [S/m]
Electrolyte effective conductivity, cathode	1 [S/m]
Current collector conductivity	5000 [S/m]
Solid effective conductivity, cathode	1000 [S/m]
Electrolyte conductivity	5 [S/m]
Electrolyte thermal conductivity	2.16 [W/m-K]
Kinetic volume, H_2	6e-6

Kinetic volume, O_2	1.66e-5
Kinetic volume, N_2	1.79e-5
Kinetic volume, H_2O	1.27e-5
Reference diffusivity	3.16e-8 [m^2/s]
Porosity	0.4

2.2.4 Numerical Techniques

In Fluent®, the default under-relaxation parameters are set to values that are near the optional largest possible number. The higher the under-relaxation factor, the faster the calculation reaches the convergence. Usually low under-relaxation factors can provide a stable iteration process. The implicit formulation is applied while the solver is set as pressure based. The SIMPLE (Semi-Implicit Method for Pressure-Linked Equations) scheme is selected to treat the pressure-velocity coupling, and the discretization scheme is chosen as the "standard" for the pressure and "first order upwind" for the momentum and energy fields. With these we solve for hydrodynamic and energy equation for temperature profiles.

For the electrochemical simulations it is brought into COMSOL® with SOFC module. As we assumed the steady state simulations, the analysis type for Maxwell-Stefan's and Navier-Stokes are set to stationary in COMSOL®. The parametric solver is used for running the electrochemical simulations. A direct (PARDISO) method is used as the linear system solver with a tolerance value of 1.0E-6. With these values we solve for the voltage, current density and species concentrations.

2.2.5 Grid Independency

A grid independent study is performed by increasing the mesh density for the single channel case. The results are shown in Fig. 2.5. In this case the SOFC works at 1083K operating temperature. As the mesh density increases, the numerical results of temperature approach to converged value. Based on the results of this grid independent study, the element size of the third case with 188,000 elements is selected for further mesh generation for other cases.

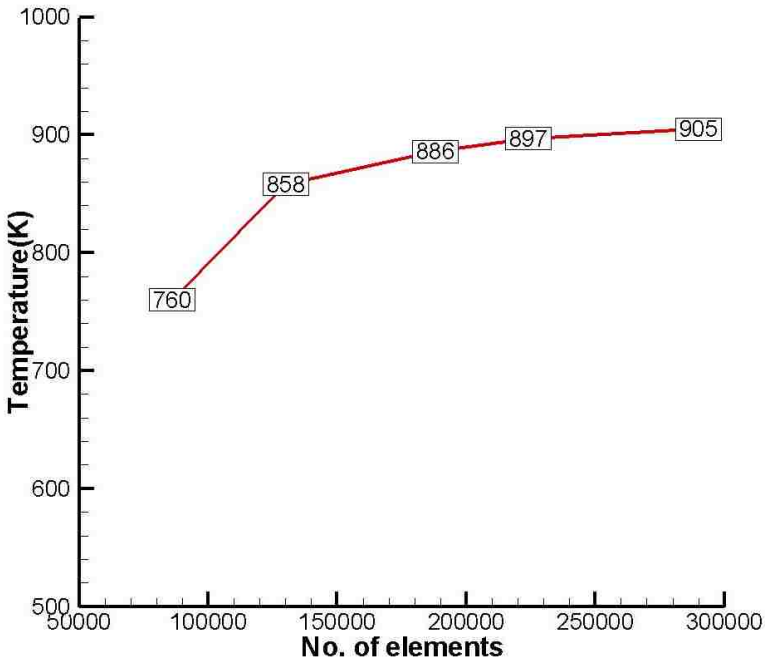

Fig. 2.5 Grid Independent Study

2.3 SOFC Model Validation

Numerical simulations were performed for the single channel solid oxide fuel cell using COMSOL® software with all the parameters stated above in Table 2.2 under several cases with different operating temperatures and counter flow types. Each simulation has obtained a converged solution. Based upon this the current density-voltage

(j-V) curves are drawn, as this j-V curve is one of the SOFC's important characteristics, which shows the fuel cell's performance under certain operating conditions.

Fig 2.6 shows the comparison between the present three-dimensional model and the research work done by Yakabe et al. [9] at 1073K. From the figure, it can be seen that, the simulated j-V curve shows good agreement with the compared published data. This good agreement indicates that the current SOFC model has been validated by Yakabe et al's published work.

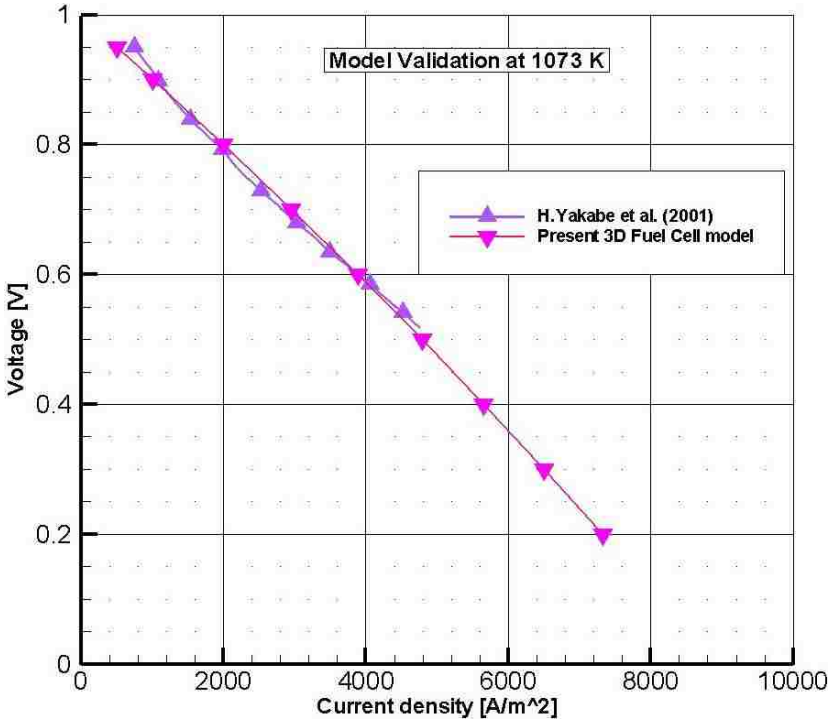

Fig 2.6 Comparison of j-V curves with published data

Fig 2.7, Fig 2.8 and Fig 2.9 show the oxygen, hydrogen and water mass fractions. From these figures and from equation (2-3) it is evident that as we move from the inlet there is species degradation for hydrogen and oxygen and there is a water production at the anode.

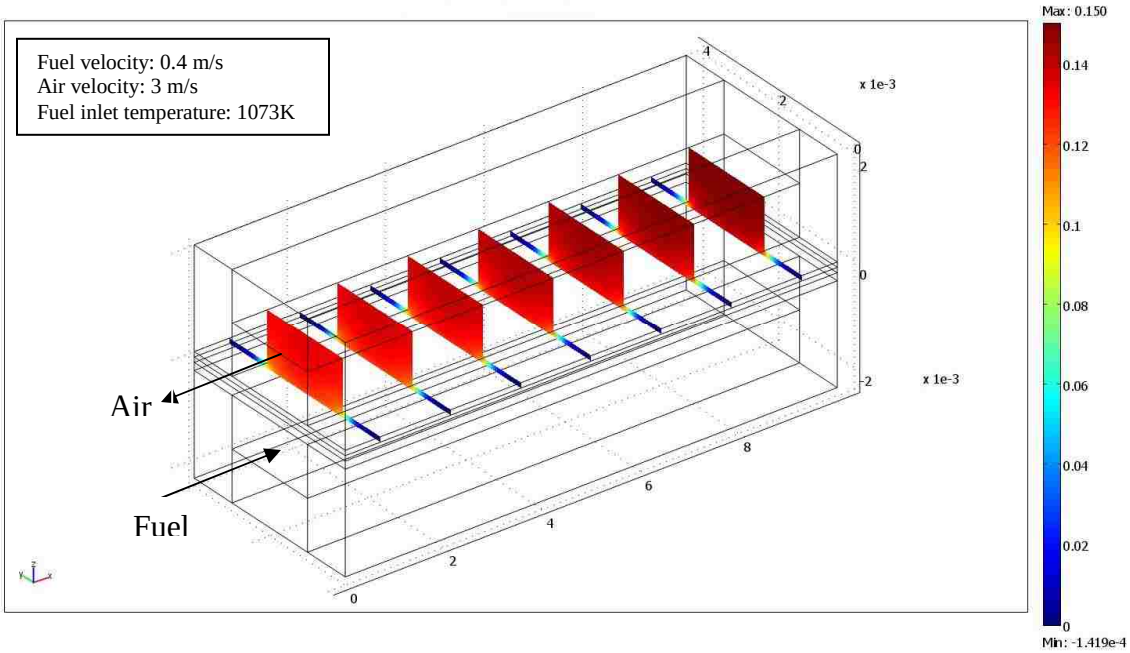

Fig 2.7 Oxygen Mass Fraction

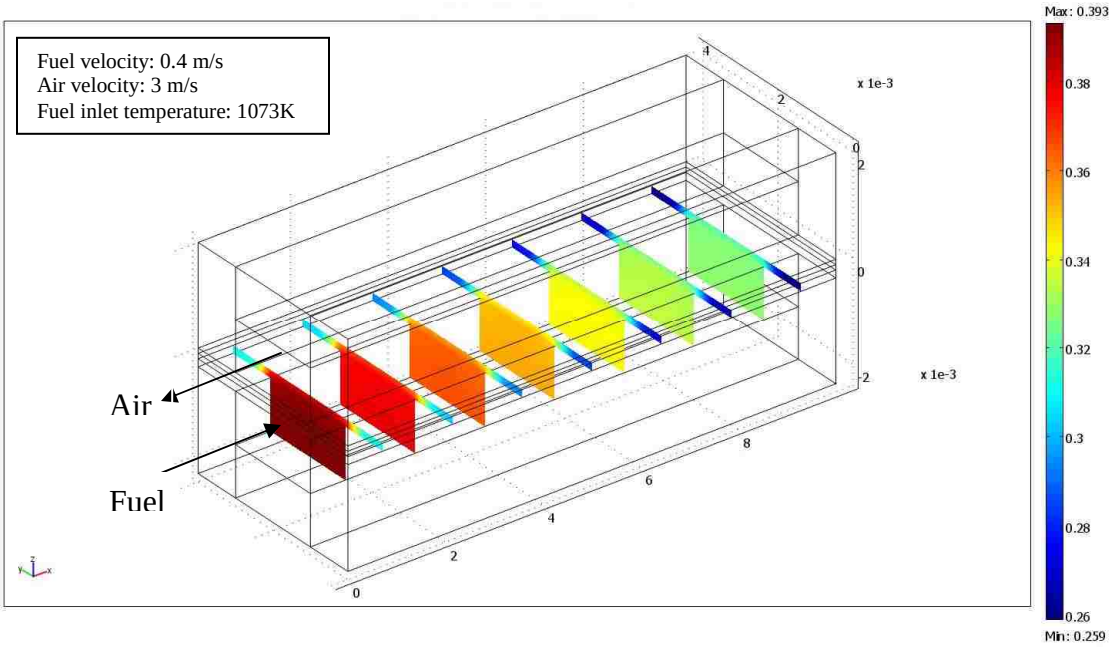

Fig 2.8 Hydrogen Mass Fraction

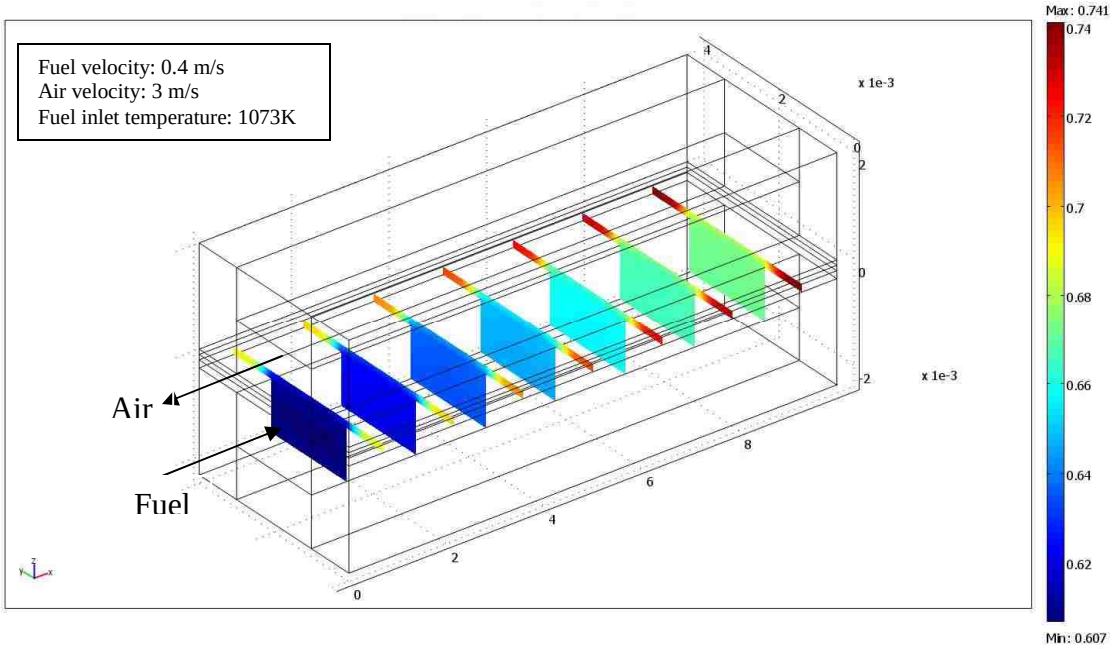

Fig 2.9 Water Mass Fraction

CHAPTER 3

NUMERICAL MODELING FOR DIFFERENT INTERCONNECT DESIGNS

In this chapter, a three-dimensional model has been developed in order to investigate the effect of interconnect design on electrical performance and degradation process. Numerical results are discussed to evaluate the performance of different kinds of SOFC interconnect designs. The current density and temperature distributions within the fuel cell have been studied. Depending on the above results the SOFC interconnect design has been optimized for better electrical performance and higher thermal stability.

3.1 Interconnect Design Description

In the planar configuration, interconnect plays a critical role. It is the element which ensures an electrical bond between cells and supplies reactive species on the electrodes. The experimental investigations have shown that interconnect decreases fuel cell electrical performance and cell durability [13]. Optimizing the interconnect design assures the better performance and stability of the fuel cell. Fig. 3.1 shows front views of the different interconnect designs which have been considered for the analysis in this thesis. These vary according to the percentage contact area of the interconnector rib with the electrodes. Here, a 0% contact area denotes a fuel cell with no interconnect rib. The anode supported design is considered to reduce the ohmic and activation losses which will incur for electrolyte support and cathode support respectively. Moreover, the anode has Ni doped in it which acts as catalyst for the reaction.

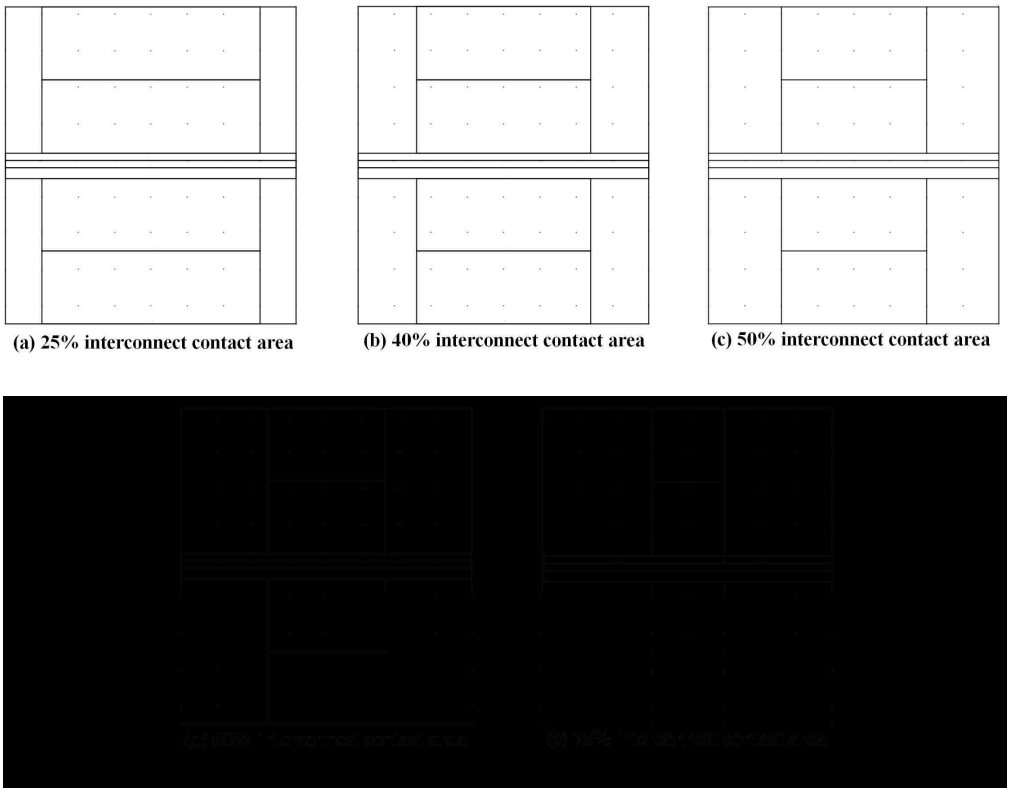

Fig. 3.1 Different interconnect designs

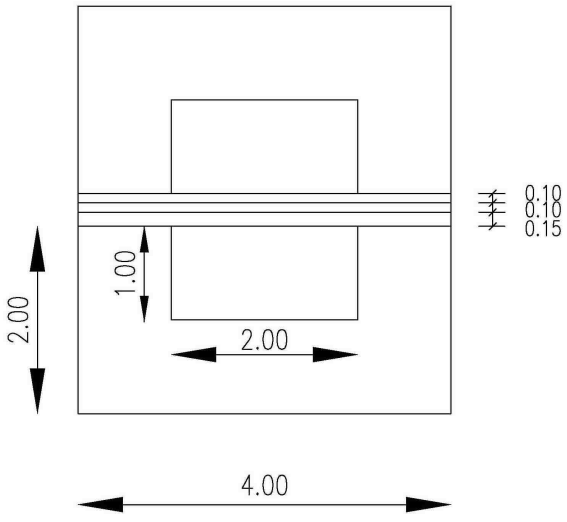

Fig.3.2 Dimensions of the interconnect design for 50% contact area (units: mm)

Fig.3.2 shows the dimensions for the design cases with 50% interconnect contact area. The dimensions of the fuel cell are the same considered above for validation. The

different designs are obtained by varying the contact surface of the interconnect rib with the electrode. In the present thesis, five different design cases are considered and optimization among them is studied. The percentage contact surface is defined as the amount of area covered by the interconnect rib on the electrodes. The different design cases considered are 25%, 40%, 50%, 60% and 75% which are shown in Fig.3.1.

Fig. 3.3 shows the computational mesh for 50% interconnect contact area which has been developed in COMSOL®. To simulate the different application modes which includes electronic conductive media, ionic conductive media, Maxwells-Stefan's diffusion and convection for anode species, Maxwells-Stefan's diffusion and convection for cathode species and weakly compressible Navier-Stokes equation, a very large memory is needed. To reduce the computational time and memory storage the size of the mesh is decreased to its minimum for which a converged solution is obtained.

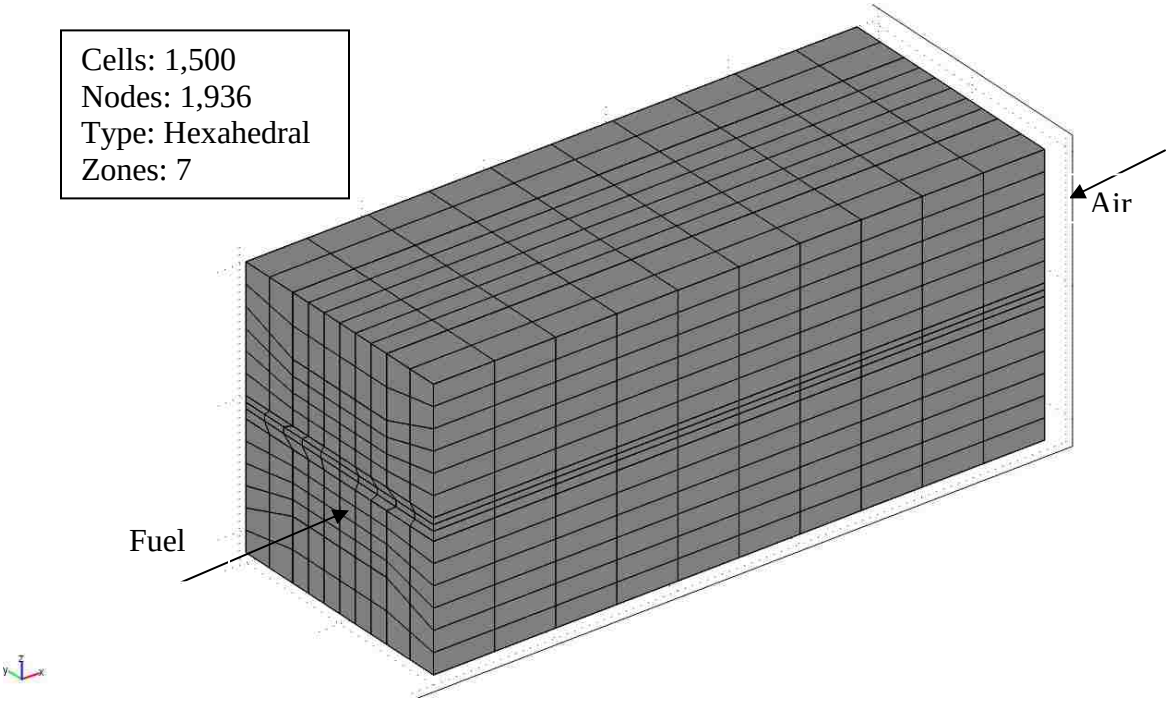

Fig.3.3 Computational mesh for 50% interconnect contact area

3.2 Operating and Boundary conditions

The commercial CFD software Fluent® and COMSOL® are used for our simulations as computational tools. Hydrodynamic and heat transfer simulations are performed using Fluent® and electrochemical simulations are done in COMSOL®. All the electrochemical parameters and the boundary conditions are specified the same as the validated SOFC model.

1) Velocity inlet

The velocity of the air at the cathode is much higher compared to the velocity of the fuel (hydrogen), this is due to the fact that the oxidation of hydrogen is fast compared with the reduction of oxygen. So, to compensate, more oxygen is supplied within the laminar region. One more advantage of having high mass flow or the high velocity is that it can keep the fuel cell within the operating temperature range. Here, in the present simulations the air and hydrogen velocities are 3 m/s and 0.4 m/s with corresponding Reynolds numbers of 230 and 16, respectively.

2) Thermal boundary conditions

The fuel inlet temperature is taken as 800^{o}C (1073K) and the reaction heat ($\dot{q}$) at the electrolyte due to the chemical reaction is given a value of 10E5 W/m^{3}. All the walls are considered to be adiabatic. Conduction is dominant within the solid materials and convection is dominant within the gas channels.

3) Species boundary conditions

The reference anode gas channel inlet mass fractions of the species are taken 0.4 and 0.6 for hydrogen and water, respectively, at the cathode gas channel 0.15, 0.37 and 0.48 for oxygen, water and nitrogen, respectively. All the outlets are considered

as convective fluxes. The effective diffusion for the species is taken in the electrodes and normal diffusion for the gas channels.

4) Charge transport boundary condition

For electronic conductive media the anode is grounded whereas the cathode is given the cell potential. All the other parts of the fuel cell are electrically insulated for ionic conductive media.

3.3 Results and Discussions

Converged numerical results were obtained for all the design cases. The heat transfer and electrochemical phenomena are investigated for the counter-flow type. The hydrogen/oxygen mass fraction and current density distribution are also examined. The pressure drop along the channel for all the interconnect design cases was calculated analytically [1] and compared with the numerical solutions.

$$\frac{dp}{dx} = \frac{2}{D^2{}_h} f \,\mathrm{Re}_h \,\mu \bar{u} \tag{3-1}$$

$$f \,\mathrm{Re}_h = 24\left(1 - 1.355\alpha^* + 1.9467\alpha^{*2} - 1.7012\alpha^{*3} + 0.9564\alpha^{*4} - 0.2537\alpha^{*5}\right) \tag{3-2}$$

where f is the friction factor, D_h is the hydraulic diameter, Re_h Reynolds number, α^* is the aspect ratio of the channel cross section, μ and $\bar{u}$ are the viscosity and mean velocity of the flowing fluid in the gas channel.

Table 3.1 shows the similarity between the numerical and analytical outcomes with an error percentage less than five. This conveys closeness of the numerical solution with the analytical real model. Also, Table 3.1 reveals the fact that numerical model always over predicts the actual results.

Table 3.1 Pressure drop along the channel

Interconnect contact area	Numerical model (Pa)	Analytical solution (Pa)	Error %
25%	87.6	83.46	4.49
40%	93.5	89.34	4.70
50%	100	95.62	4.61
60%	111	106.46	4.26
75%	155	150.27	3.14

3.3.1 Temperature Distribution

The temperature graphs were drawn for the fuel cell along middle length of the electrolyte/anode interface for all the different interconnect design cases using the Fluent®. The temperature difference between the fuel inlet and air inlet are calculated and tabularized in Table 3.2 for all the design cases.

Table 3.2 Temperature difference between fuel inlet and air inlet at electrolyte/anode interface

Design Cases	Temperature Difference
25% interconnect contact	47K
40% interconnect contact	43K
50% interconnect contact	40K
60% interconnect contact	37K
75% interconnect contact	26K

Fig.3.4 shows the temperature graphs for different interconnect contact area. From Table 3.2 and Fig.3.4 it is evident that as the interconnect contact area increases the temperature difference between fuel inlet and air inlet is decreasing effectively. The increase in the interconnect area decreases the active surface for the electrochemical reaction. As the overall reaction is an endothermic and the reaction heat is proportional to the reaction site area there will be decrease in the temperature difference for increase in the interconnect contact area. The temperature at a point on the electrode/electrolyte interface at the fuel inlet is around 925K for all the design cases.

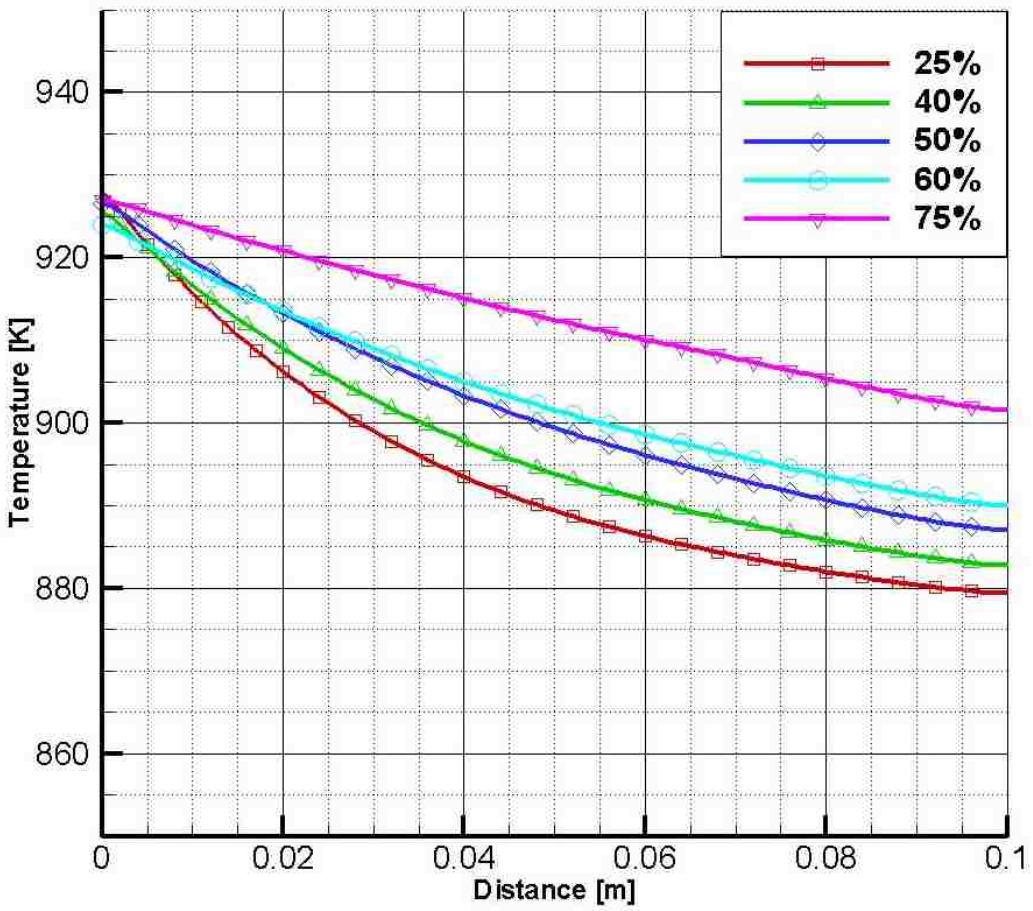

Fig.3.4 Electrolyte/anode interface temperature distribution

3.3.2 Polarization Curves

Polarization curves are also known as performance curves estimates the fuel cell performance in terms of voltage, current density and power density factors. From Fig.1.2 in Chapter One it can be noticed that current of the fuel cell increases as the voltage decreases. This is because power equals to voltage times the current. Therefore, current and voltage are inversely proportional. The better the fuel cell, the closer to zero is the slope of the polarization curve.

3.3.2.1 Current Density

The current density of the fuel cell reflects its performance and how much power it provides to the outside circuit. The electrochemical simulations were performed for all the above described interconnect design cases using the COMSOL® multi-physics and the current density profiles were plotted. Fig. 3.5 shows the current density and voltage (j-V) curves for all the interconnect design cases.

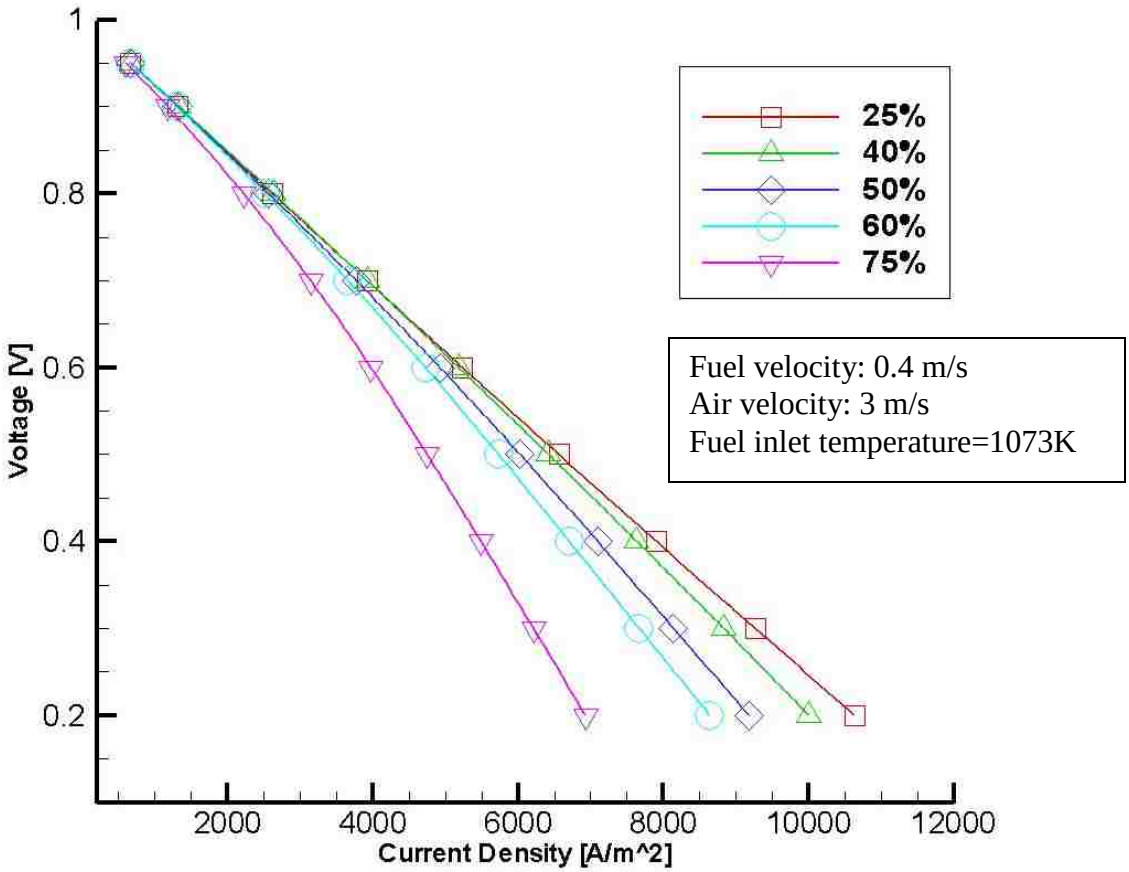

Fig.3.5 Current density versus voltage curves

From Fig.3.5 it can be seen that at high working temperatures of SOFCs, the activation losses are minor. In SOFC major losses are dominated by ohmic resistance offered by the electrolyte [34], and this is evident from the obtained j-V curves. For large active area at 25% interconnect contact area the concentration losses are minimal and it is gradually increasing with the increase in the interconnect contact area. Further, there is decrease in the ohmic overvoltage with the increase in the interconnect contact area. As the channel width decreases the active diffusion surface area also decreases, thereby causing difficulty for the species to diffuse through the porous electrodes. It is also even difficult to remove the product species making mass transport losses dominate the fuel

cell performance. From Fig.3.5 it is seen that with the increase in the interconnect contact area there is substantial decrease in the current density within the operating voltage. This establishes the importance and the effect of the interconnect design for a fuel cell.

3.3.2.2 Power Density

Power density curves directly give the maximum power which can be obtained for a specified fuel cell. As power is equal to product of current and voltage, it is very easy to get the power density plots for a given fuel cell. From Fig.3.6 and Fig.3.7 the trend follows the same pattern with the increase in the interconnect contact area there is decrease in the power density. The highest power density recorded at 0.6V operating voltage is 3142.8 W/m^2 for the 25% interconnect contact area and the lowest is for the 75% interconnect contact area with a value of 2385.72 W/m^2. So, from the calculated values there is an approximate 24% decrease in the power density with the interconnect contact area increasing from 25% to 75%.

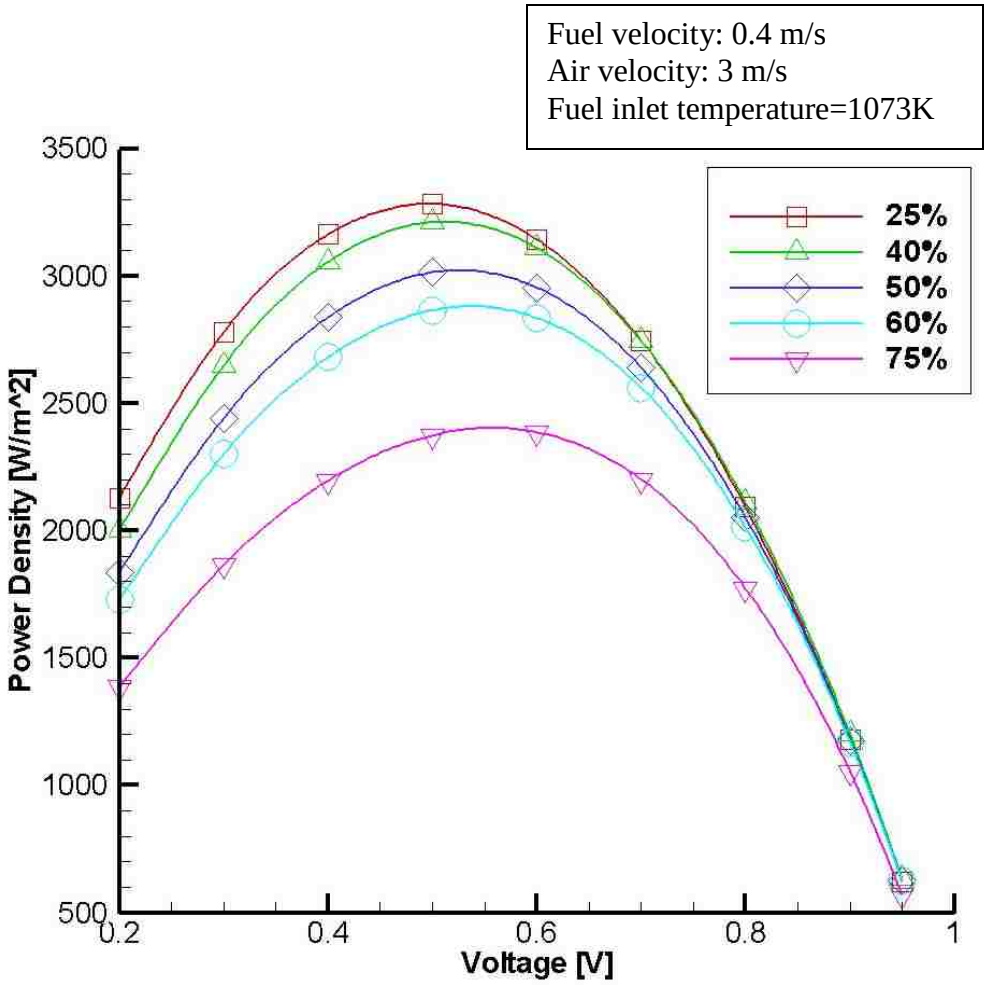

Fig.3.6 Power density versus voltage curves

The peak power densities for different interconnect contact areas are plotted in Fig. 3.8 to observe the trend of how the power density varies with the interconnect contact area. As explained above, the power density is decreasing with the increase in the interconnect contact area. This shows that the interconnect design influences the fuel cell performance significantly. So, optimizing the interconnect design is very important for SOFC performance as this aspect has a great impact on cell performance.

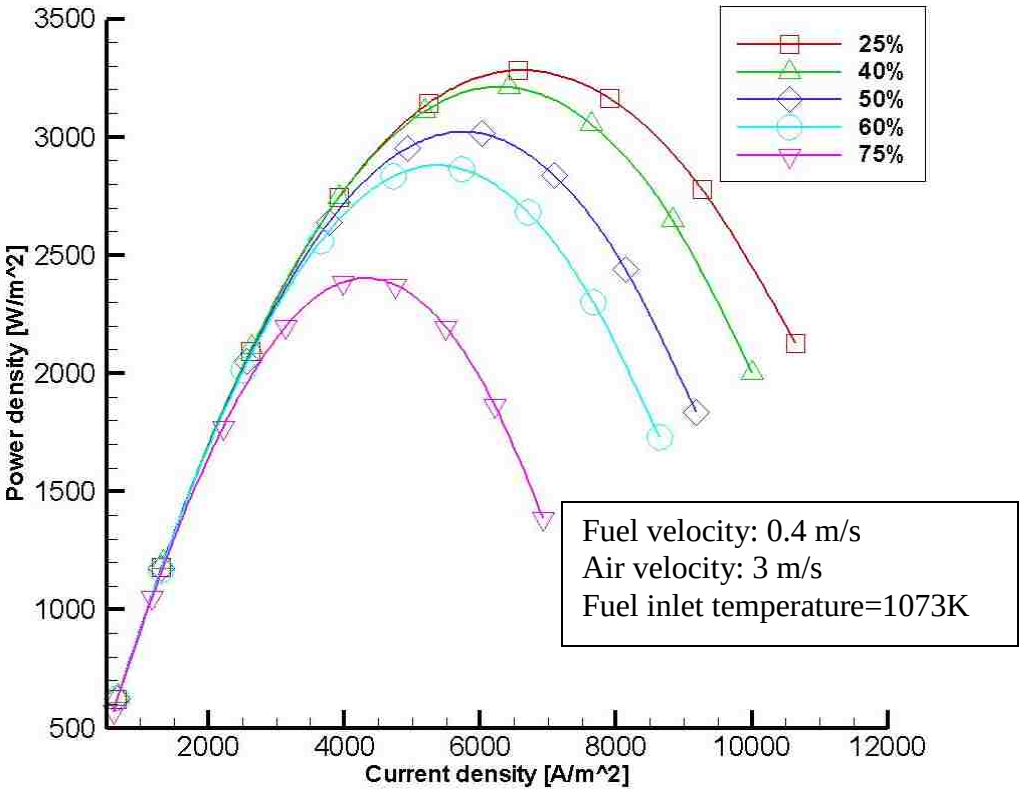

Fig.3.7 Power density versus current density curves

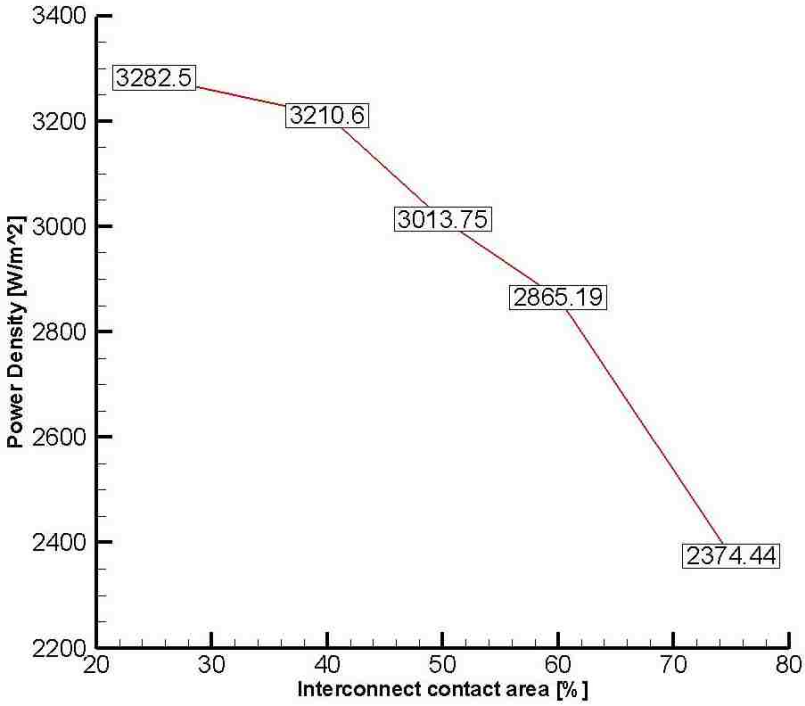

Fig.3.8 Peak power density for different interconnect contact area

3.3.3 Hydrogen Mass Fraction

Hydrogen mass fraction along the length reflects the supply of hydrogen to the fuel cell. Hydrogen fuel is supplied to the anode gas channel with an inlet mass fraction of 0.4. Fig. 3.9 shows the consumption of hydrogen along the channel length and diffusion through anode electrode from fuel inlet to the outlet for all the interconnect design cases. Hydrogen diffuses through the porous electrode to reach the reaction site and oxidize due to the chemical reaction. From Fig.3.6 (a)-(e) as the interconnect area increases the hydrogen consumption decreases which slows down the electrochemical reaction at the electrolyte/electrode interface. The amount of reaction is proportional to the number of electrons harnessed through the external circuit. So, it is evident from the above polarization curves that power density decreases with increase in the interconnect area.

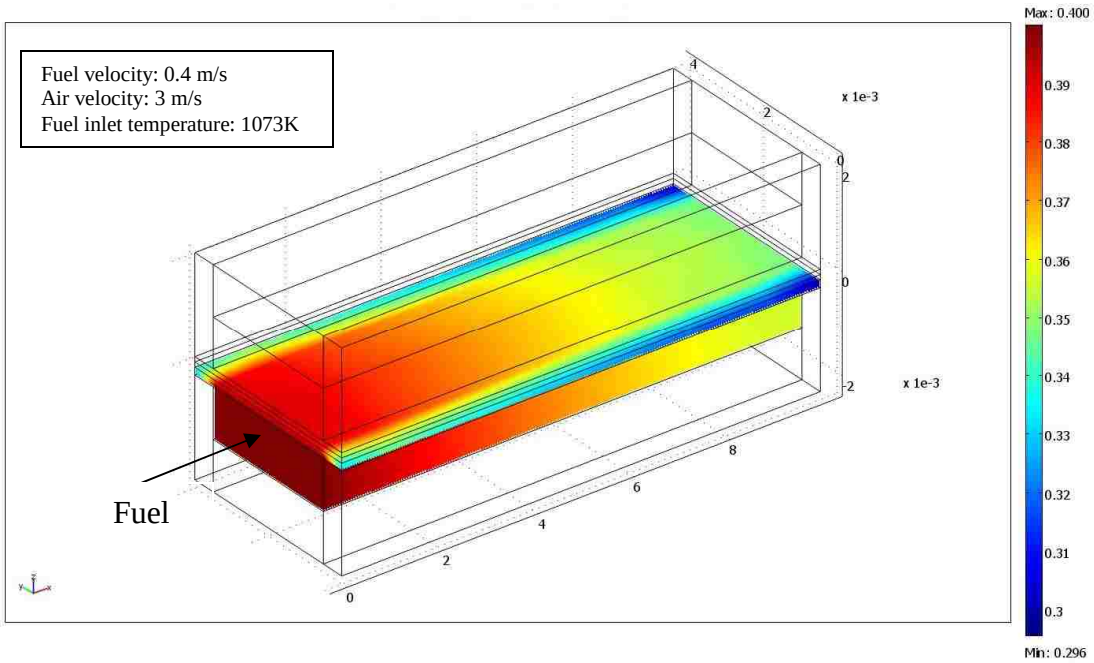

(a) 25% interconnect contact area

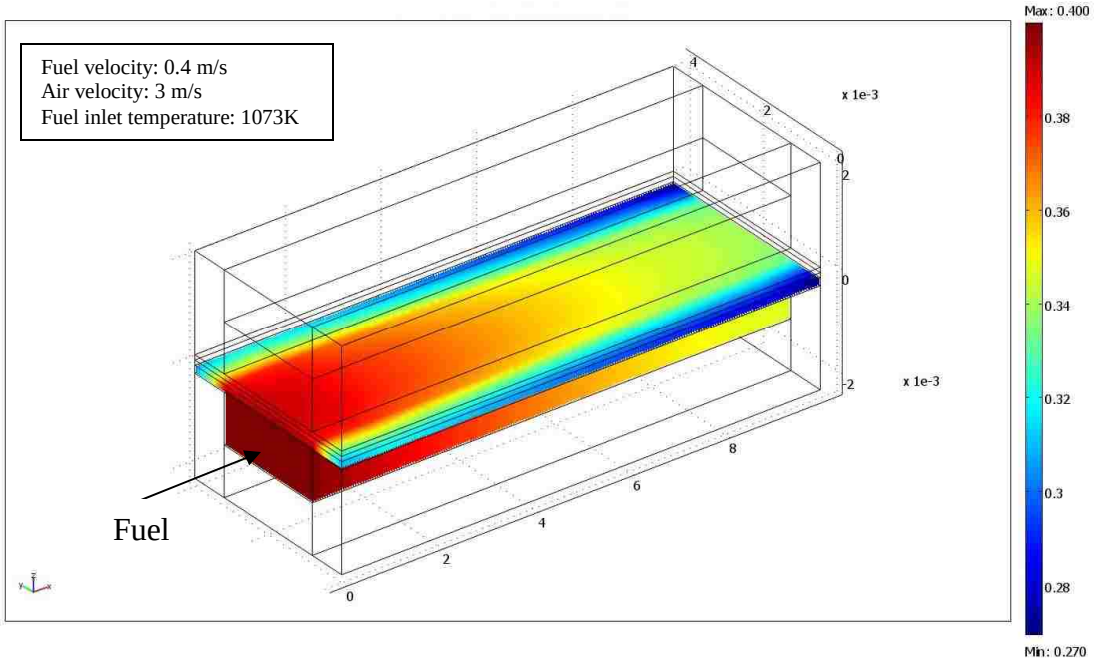

(b) 40% interconnect contact area

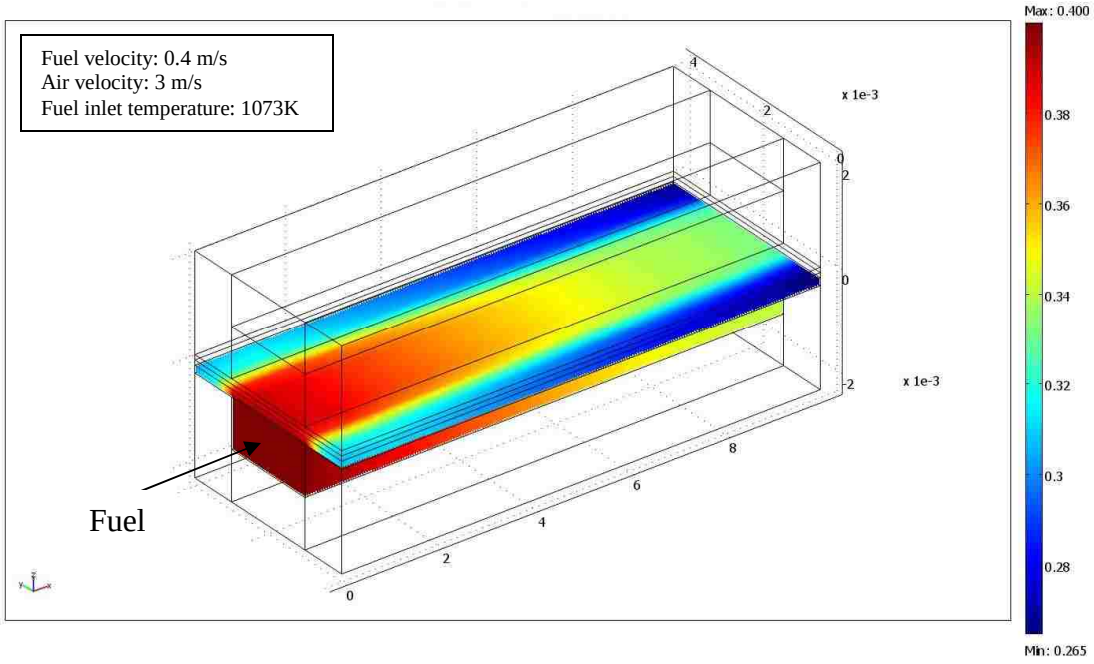

(c) 50% interconnect contact area

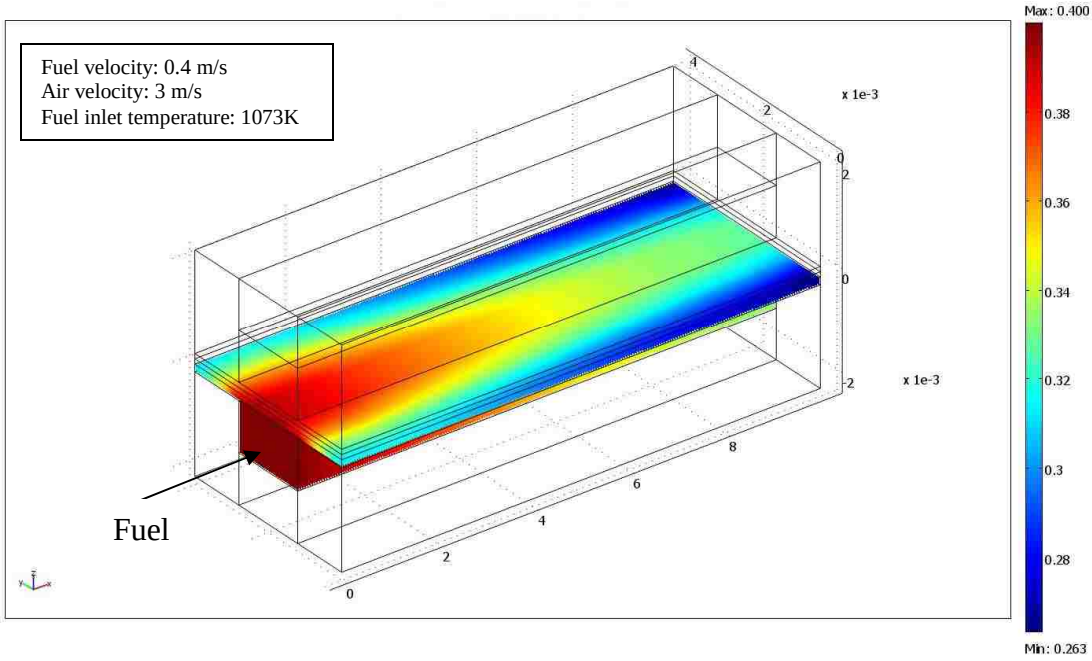

(d) 60% interconnect contact area

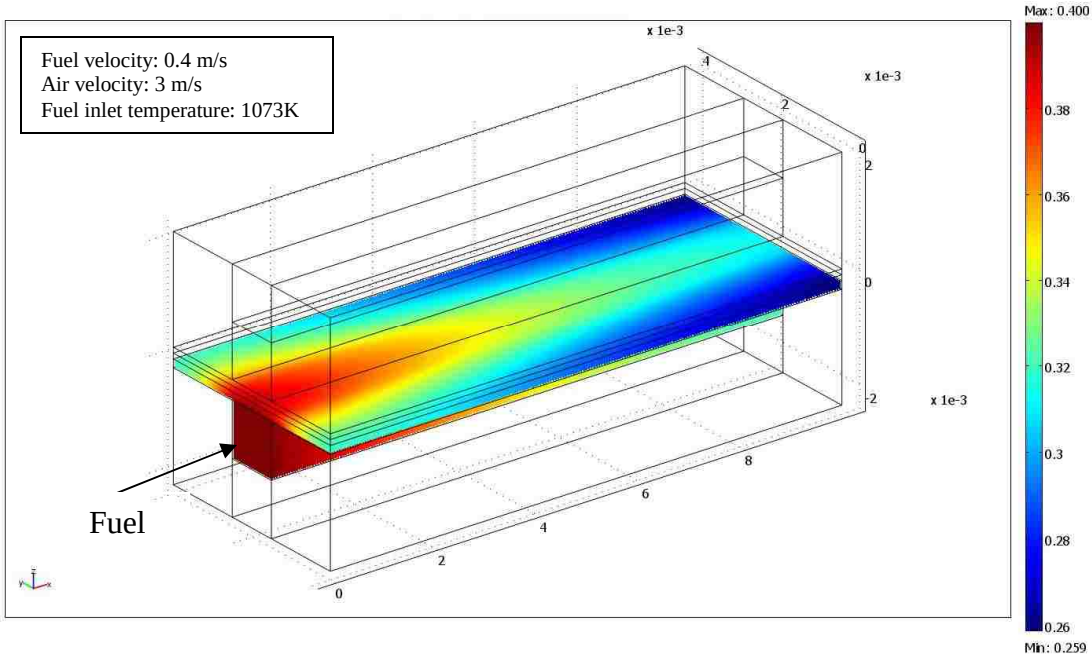

(e) 75% interconnect contact area

Fig.3.9 Hydrogen mass fraction

3.3.4 Oxygen Mass Fraction

Oxygen mass fraction along the length reflects the supply of oxygen to the fuel cell. The inlet mass fraction of oxygen supplied at the cathode gas channel is 0.15. Fig. 3.10 shows the supply of oxygen to the cathode gas channel and its diffusion through the cathode electrode for all the interconnect design cases. The mass fraction of oxygen at the air entrance is high and it gradually decreases along the channel length due to the oxygen species diffusion through porous electrodes and its reduction at the electrolyte/electrode interface. It is similar to the hydrogen mass fraction in the anode channel.

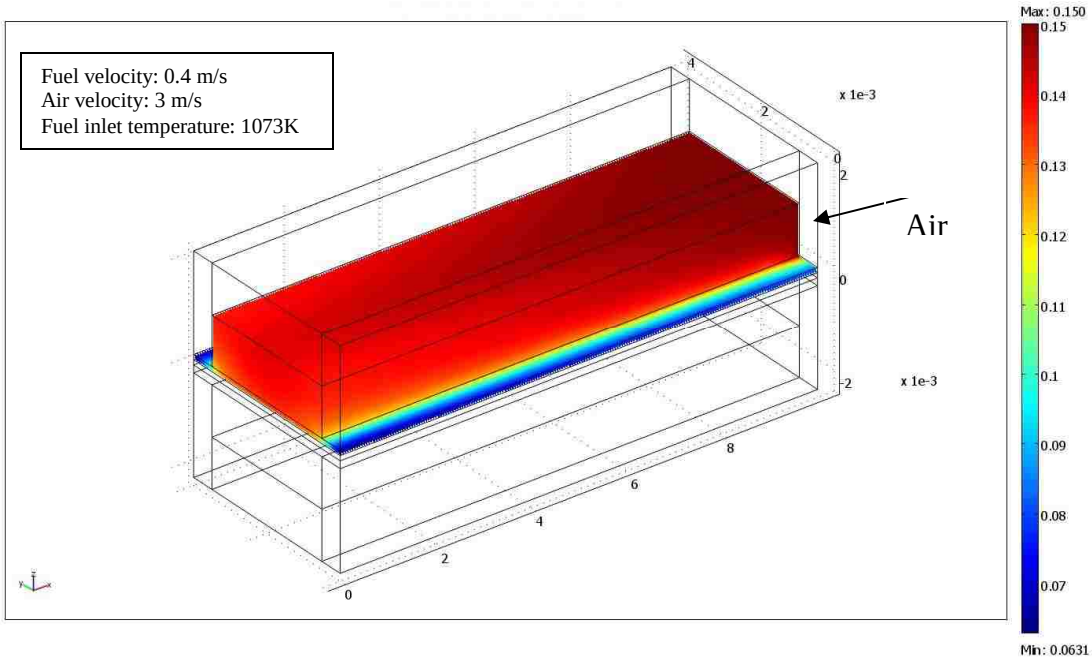

(a) 25% interconnect contact area

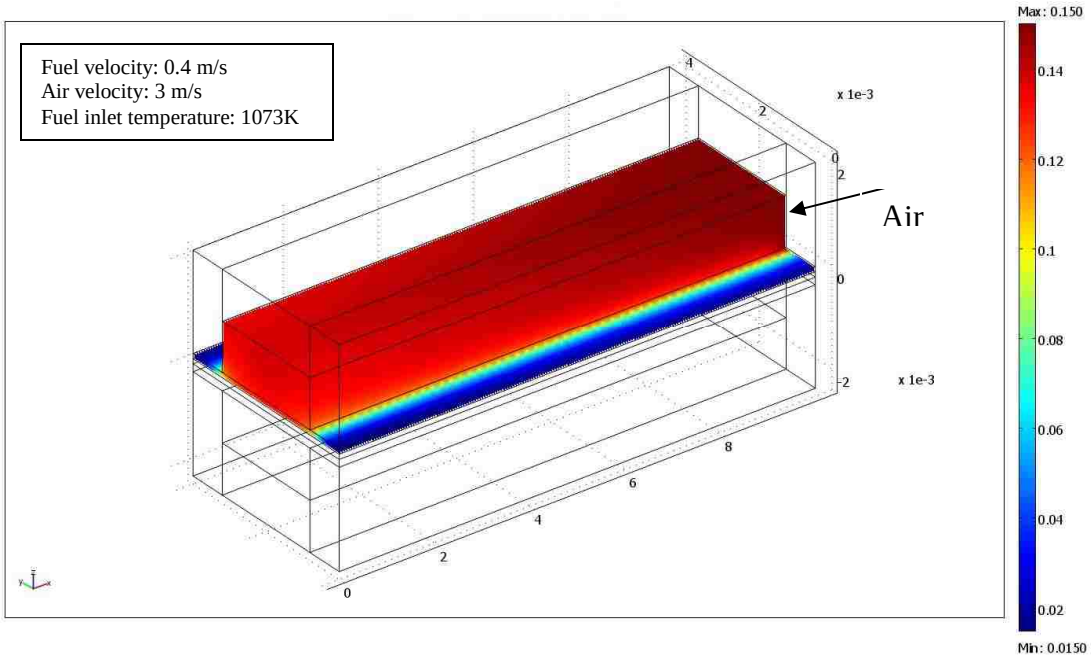

(b) 40% interconnect contact area

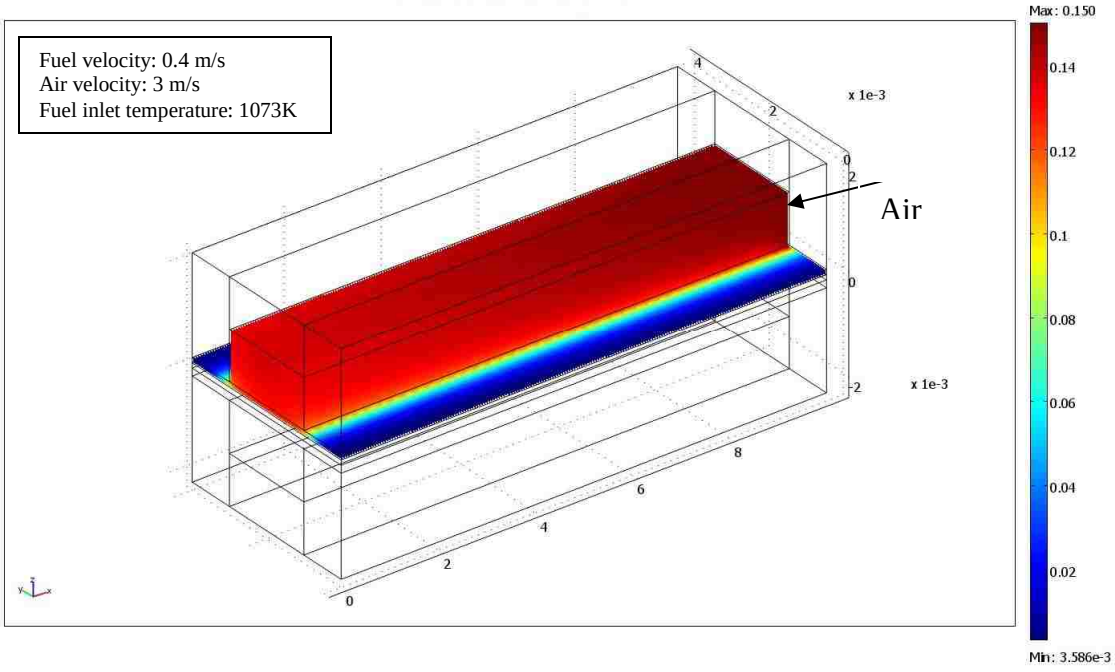

(c) 50% interconnect contact area

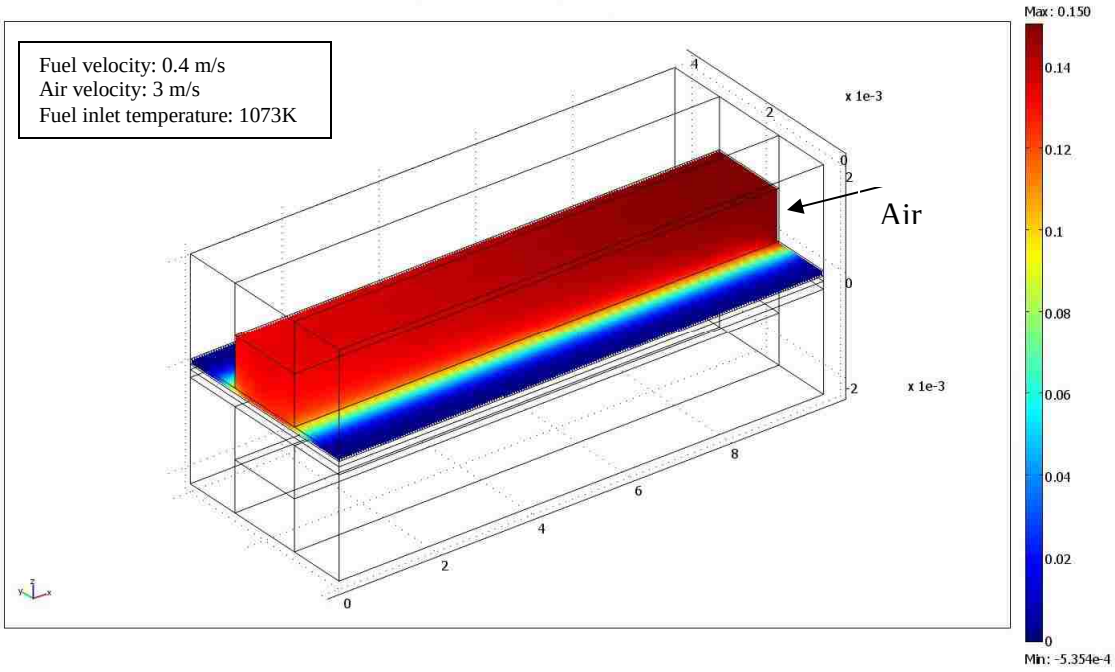

(d) 60% interconnect contact area

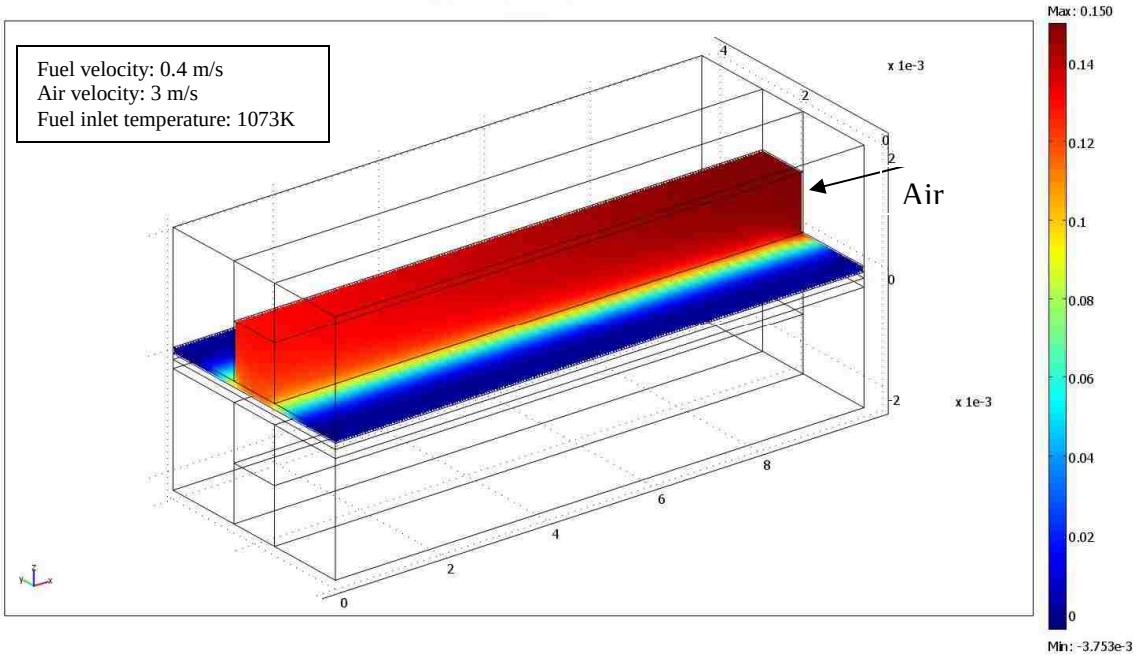

(e) 75% interconnect contact area

Fig.3.10 Oxygen mass fraction

CHAPTER 4

OPTIMIZATION OF INTERCONNECT DESIGN FOR PLANAR SOFC

In this chapter, the planar SOFC interconnect is optimized among the five different cases explained in the previous chapter, for better performance and stability of the fuel cell. For the best design the parametric study is carried out with different mass flow rates, hydraulic diameters and interconnects' material properties. From the results obtained the effect of each parameter can be clearly understood.

4.1 Interconnect Design Optimization

The results obtained from the numerical simulations for the different interconnect designs from the previous chapter allows the optimization of interconnect design for the planar SOFC. Interconnect design have been modified to reduce the thermal gradient and improve the electrical behavior. The smaller is the contact surface; the better the electrical performance (see in Fig.3.5). Nevertheless, the temperature gradients increase with decreasing contact surface (see in Fig.3.4). So, the optimization is carried out considering the temperature gradient and electrical behavior.

From Table 4.1 the best thermal behavior is recorded for 75% interconnect contact area but it has the poor electrical performance. Similarly, for 25% interconnect contact area it has the best electrical performance and failed to have good thermal behavior. It is that, for SOFC to have high current density we need to pay for the material stability. So, the optimization of the interconnect design is carefully performed to get considerable power output with long running of the fuel cell.

Table 4.1 Temperature gradient and power density for different interconnect design cases

Design Cases	Temperature Gradient [K]		Power Density [W/m^2]	
		% decrease		%decrease
25% interconnect contact	47	8.52	3142.86	1.12
40% interconnect contact	43	6.91	3109.35	5.16
50% interconnect contact	40	7.56	2953.66	4.04
60% interconnect contact	37	29.72	2834.31	15.83
75% interconnect contact	26		2385.72	

If 25% interconnect contact area is considered to be the design criteria with maximum temperature limit for the material stability, the 60% interconnect contact area has the better performance considering both thermal and electrical behaviors. At high operating temperatures thermal stresses are induced on the fuel cell materials which drastically affect the fuel cell performance. So, reducing the temperature gradient improves the operating life of the fuel cell. At the operating voltage of 0.6 V there is 4.04% decrease in the power density and 7.5% decrease in the temperature gradient are recorded for 60% interconnect contact area compared with the 50% interconnect contact area. In SOFCs the stability and degradation of the materials is very significant as they work at high temperatures. So, temperature gradient plays a vital role while defining the SOFC overall performance. For every one degree change in the temperature gradient along the length of the fuel cell impacts on the SOFC degradation process. Considering all the above statements the 60% interconnect contact surface has the better temperature gradient with considerable power density.

4.2 Parametric Study For Optimized Design

Parametric study is carried out for the optimized 60% interconnect design case for different mass flows, hydraulic diameters and interconnects material properties. The results allow having the fuel cell with the best performance.

4.2.1 Mass Flow

For the optimized 60% interconnect design the results were plotted for different mass flows inlets. This is carried out by changing the velocity for the fuel inlet at the anode gas channel. Mass flow rate at the anode gas channel is important because it affects the economics of the fuel cell in terms of fuel consumption. Fig.4.1 shows the current density and power density plots for velocities 0.4 m/s (Re=16), 0.6 m/s (Re=21), 0.8 m/s (Re=25) and 1 m/s (Re=31), respectively.

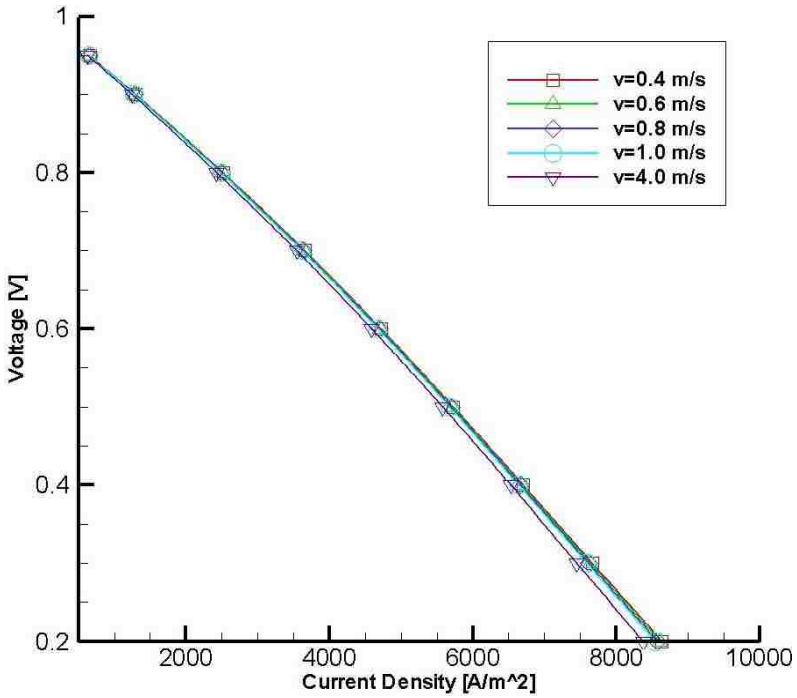

(a) Current density

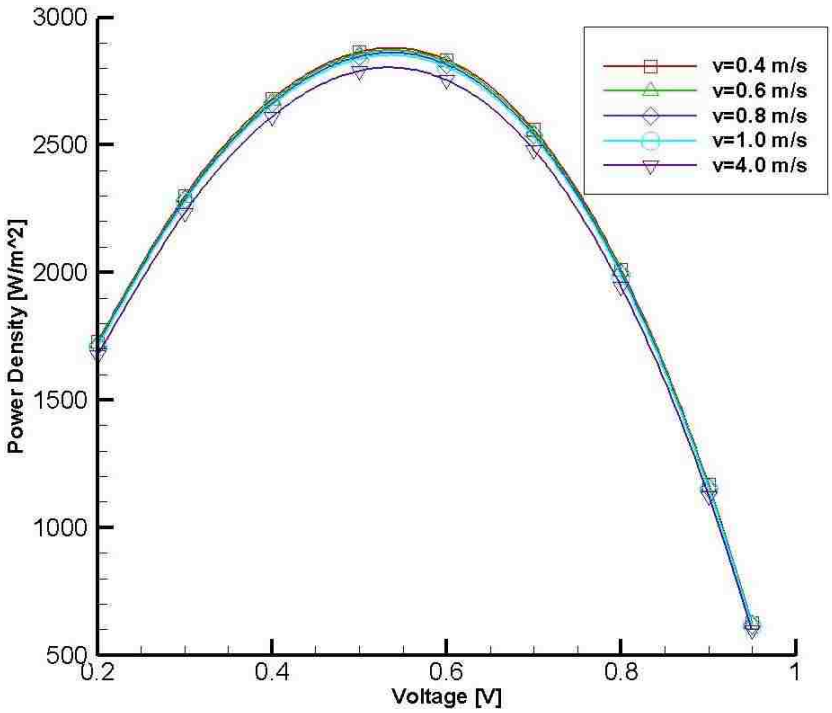

(b) Power density

Fig.4.1 Polarization curves for 60% interconnect design for different mass flows rates

From the above plots, it can be seen that the power density decreases with an increase in the velocity. In general increasing the gas flow velocity will improve the mass transport situation along the length of the flow channel. This effect of velocity also increases the temperature of the fuel cell which has the direct effect on the open circuit voltage from equation (1-7). It can be seen that at 0.6 V operating voltage as the velocity is doubled from 0.4 m/s to 0.8 m/s there is 0.66% decrease in the power density and 2.83% decrease in the power density for the velocity change from 0.4 m/s to 4.0 m/s.

Fig.4.2 shows the mass fraction of hydrogen at the anode gas channel and anode electrode. From the contours it can be seen that as the velocity increases the mass fraction of hydrogen also increases.

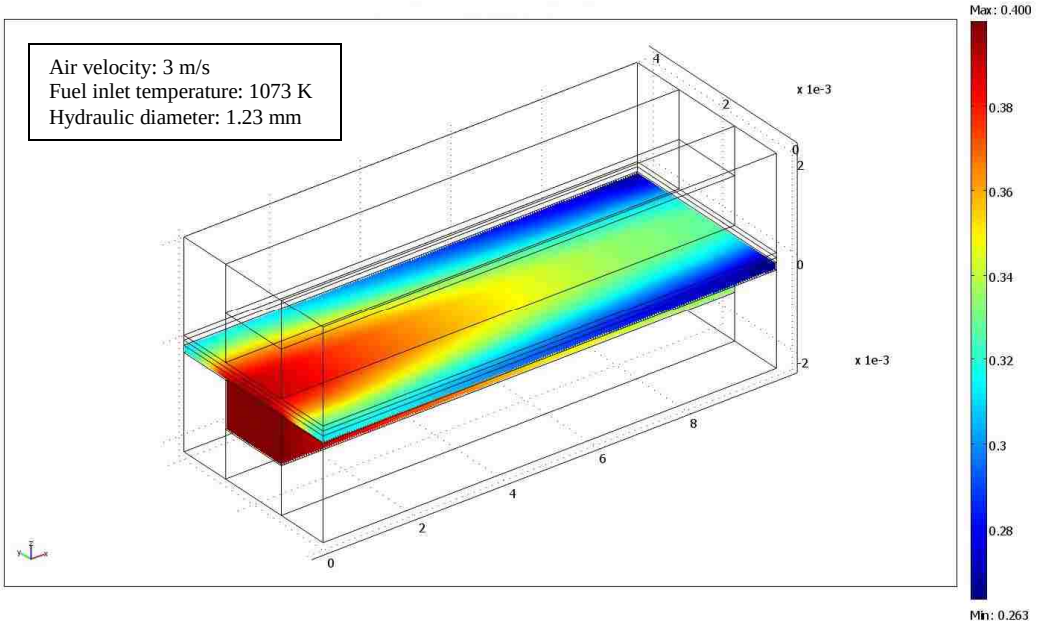

(a) Mass fraction of hydrogen at v=0.4 m/s

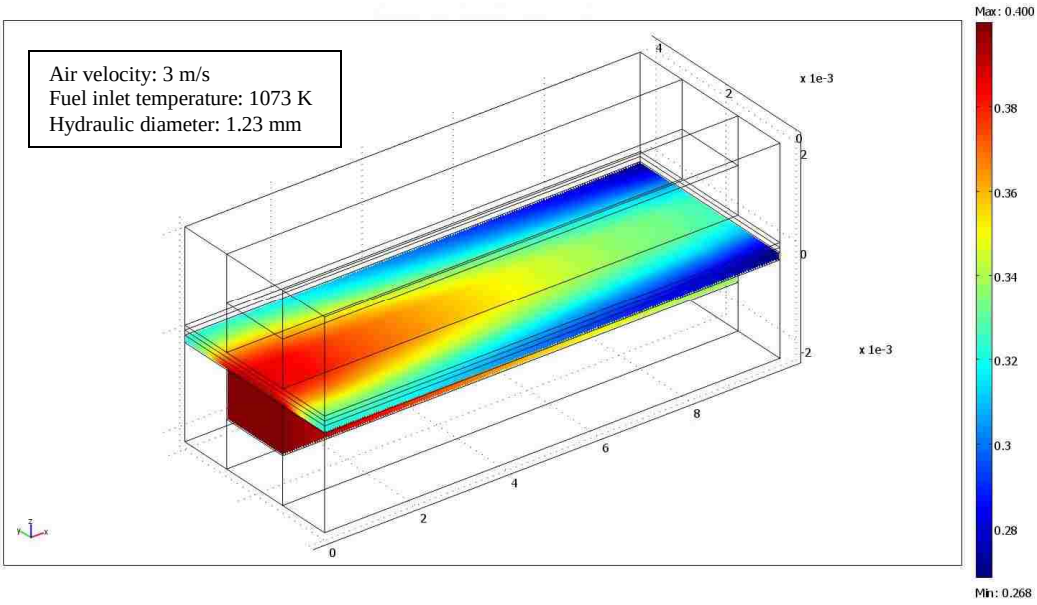

(b) Mass fraction of hydrogen at v=0.6 m/s

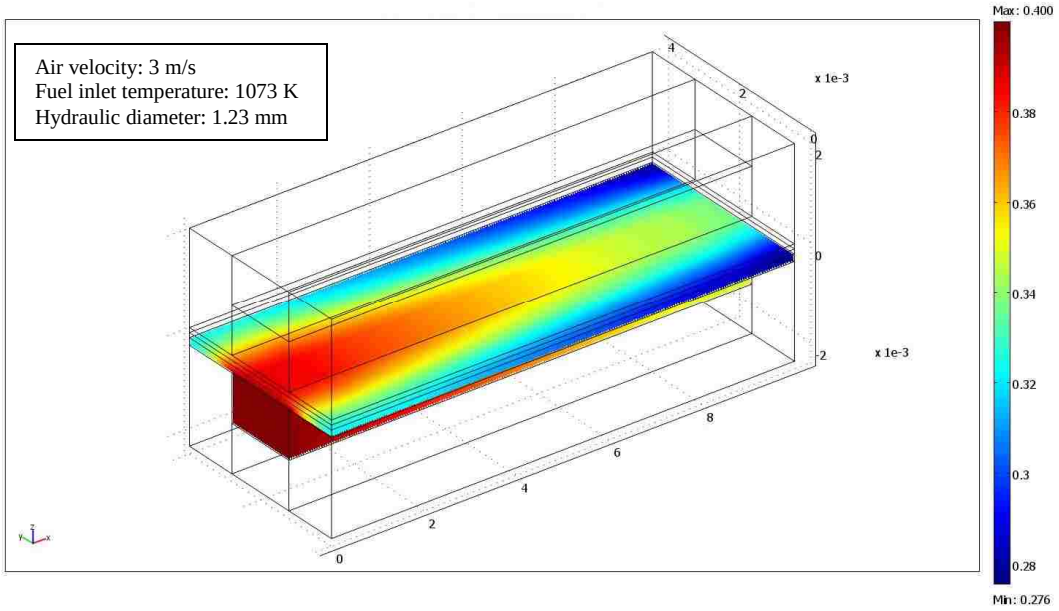

(c) Mass fraction of hydrogen at v=0.8 m/s

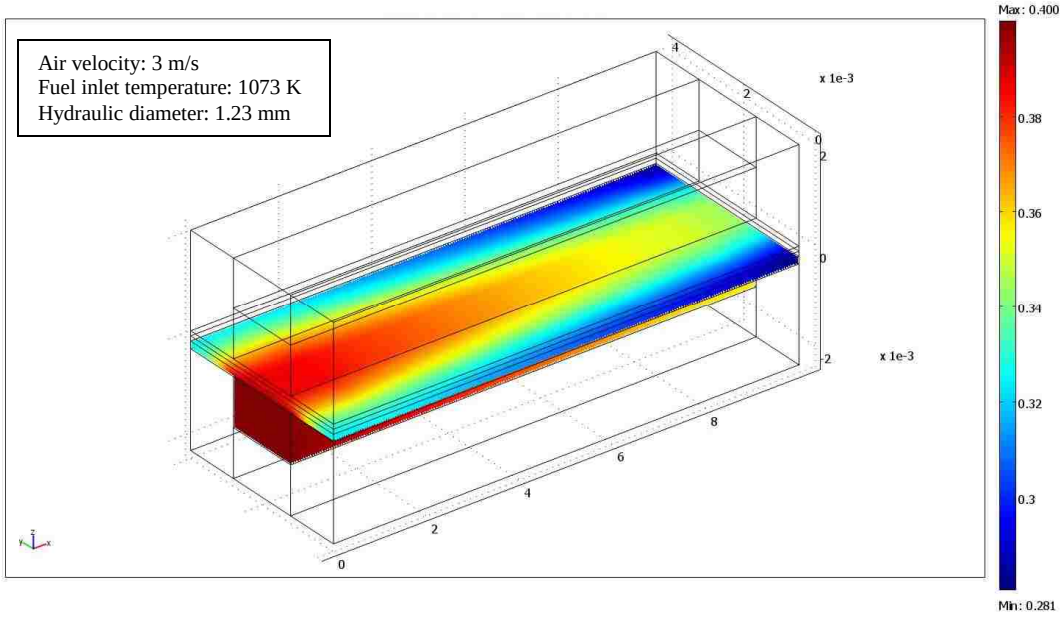

(d) Mass fraction of hydrogen at v=1.0 m/s

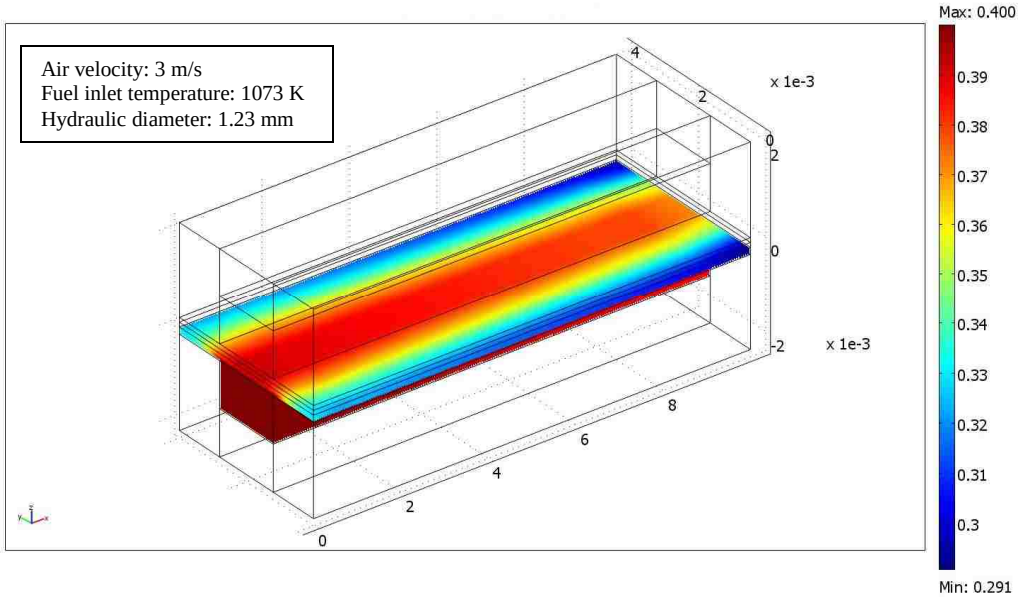

(e) Mass fraction of hydrogen at v=4.0 m/s

Fig.4.2 Mass fraction of hydrogen for different mass flow rates for 60% interconnect design

4.2.2 Hydraulic Diameter

The hydraulic diameter D_H is a commonly used term when handling flow in noncircular tubes and channels. It is defined as

$$D_H = \frac{4A}{P} \tag{4-1}$$

where A is the cross sectional area and P is the wetted perimeter of the cross-section.

The optimized 60% interconnect design has the hydraulic diameter 1.23 mm. Simulations were performed for D_H =1 mm and D_H =1.5 mm to investigate the effect of it on the electrical performance of the fuel cell. Fig.4.3 gives the clear picture of the different hydraulic diameters used in this chapter. These are formed by changing the height b for the gas channel.

The anode gas channel velocity (0.4 m/s) is kept constant for all the different hydraulic diameters. Fig.4.4 explains the electrical behavior of the fuel cell for different hydraulic diameters. At the operating voltage 0.6 V, power density is increasing gradually with increase in the hydraulic diameter. Even for D_H =1 mm the flow is still in the laminar region. As the hydraulic diameter decreases for the same mass flow, pressure along the gas channel increases. This effect of pressure has small impact on the electrical performance of the fuel cell which can be found from Fig.4.4. For the change in hydraulic diameter from D_H =1 mm to D_H =1.5 mm for the same mass flow there is only 1.4% decrease in the power output. The mass flux due to the convective mass transfer for the species along the electrode thickness is given by

$$J_{C,i} = h_m\left(\rho_i - \overline{\rho}_i\right) \tag{4-2}$$

$$h_m = Sh\frac{D_{ij}}{D_H} \tag{4-3}$$

where $J_{C,i}$ is the convective mass flux (kg/m^2-s), ρ_i is the density (kg/m^3) of species i at the electrode surface, $\overline{\rho}_i$ is the mean density (kg/m^3) of species i in the bulk fluid, h_m is the mass transfer convection coefficient (m/s) and Sh is the Sherwood number.

It is clear that as the hydraulic diameter D_H increases the area also increases and for constant mass flow rate and species density the velocity decreases. The velocity is proportional to the convective mass transfer coefficient, this decrease has an effect on the convective mass flux from equation (4-2) which increases the concentration loss. This explains the decrease in the power density for the increase in the hydraulic diameter.

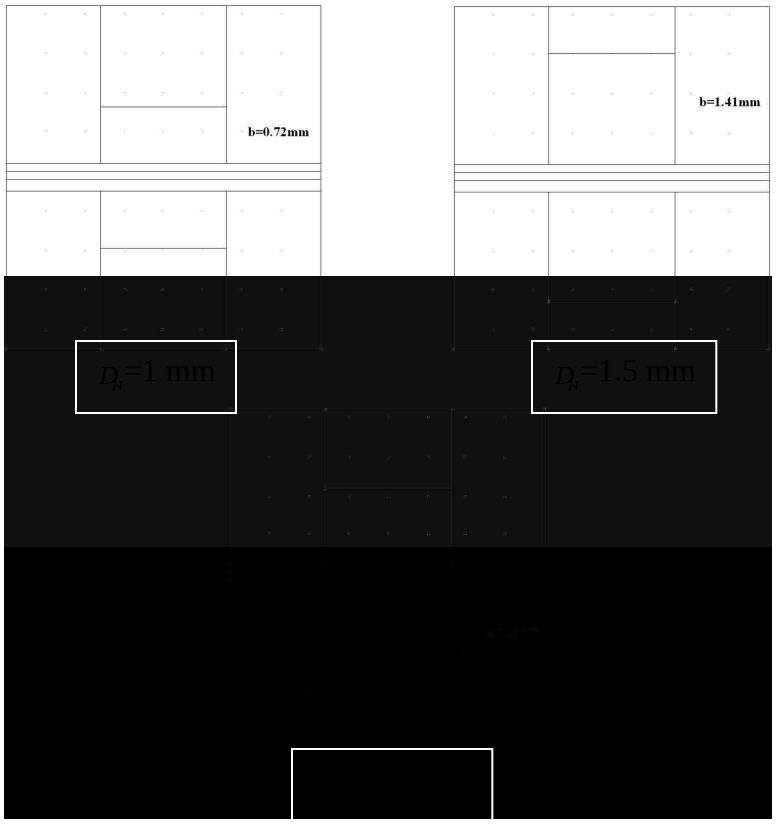

Fig.4.3 Front view of the 60% interconnect design with different hydraulic diameters

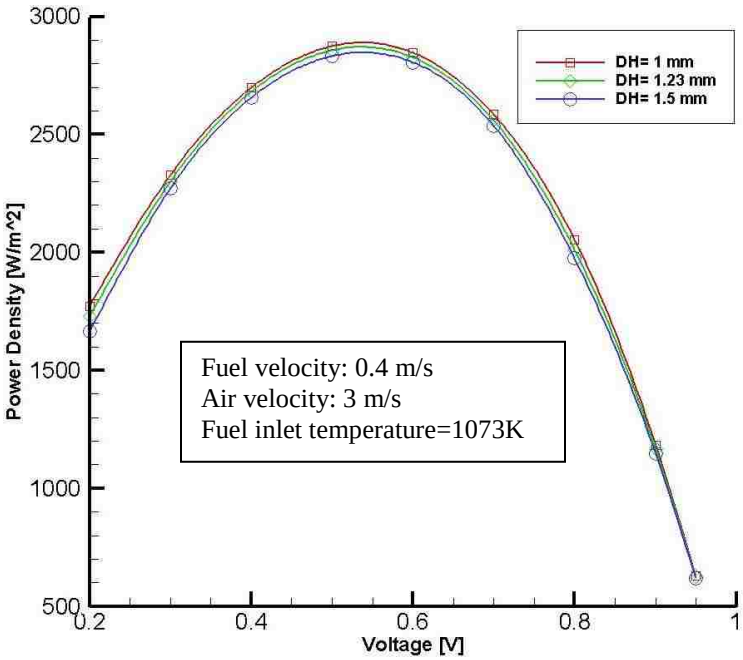

Fig.4.4 Power density curves for different hydraulic diameters

4.2.3 Interconnect Material Conductivity

Interconnect for the SOFC plays an important role; it assures the electrical connection between anode of one individual cell to the cathode of neighboring one and it harness the electrons produced from the electrolyte/electrode structure during reaction. It also acts as a physical barrier to protect the air electrode material from the reducing environment of the fuel on the fuel electrode side, and it equally prevents the fuel electrode material from contacting with oxidizing atmosphere of the oxidant electrode side.

Under the SOFC operating environment, interconnect must exhibit excellent electrical conductivity and its absolute magnitude should be reasonably large. A value of 5000 S/m for $LaCrO_3$–based solids is a well-accepted minimum electrical conductivity for the usefulness of interconnects in SOFC [35]. In the present thesis different electrical conductivity values for interconnect material have been used which are in the acceptable range. Simulations were performed for calcium doped (K_s=4500 S/m) and strontium doped (K_s= 5500 S/m) $LaCrO_3$. Fig.4.5 shows the current density and power density comparison between the different electrical conductivity values including the K_s=5000 S/m which has been used throughout our simulations. It can be seen electrical performance of the SOFC is better at high electrical conductivity values.

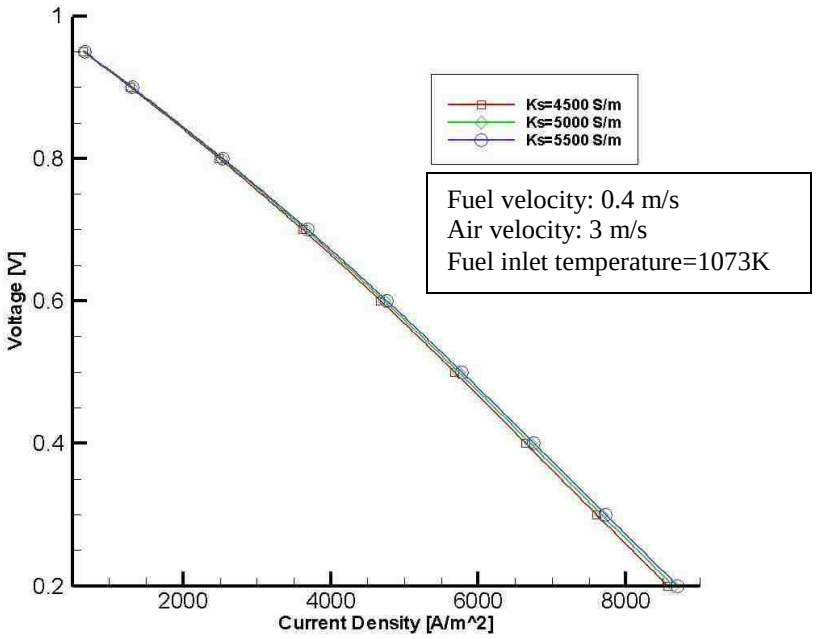

(a) Current density plots

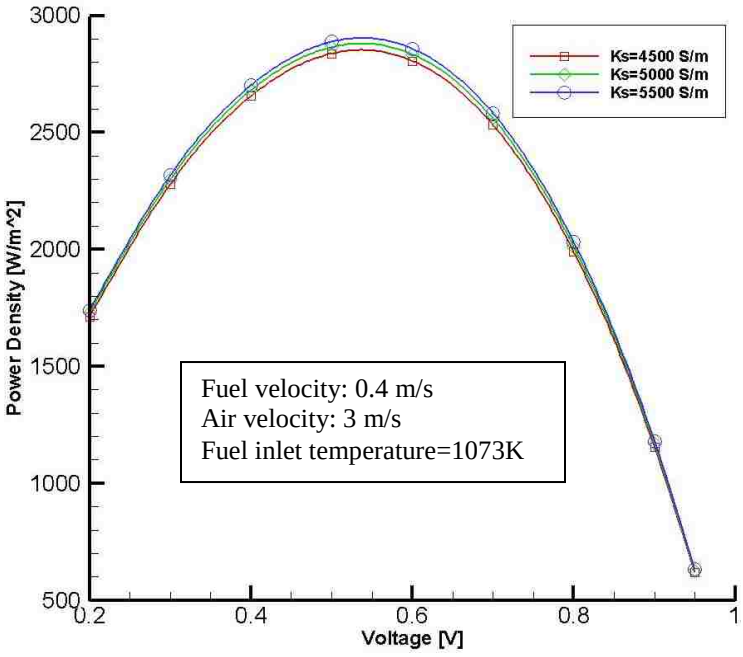

(b) Power density plots

Fig.4.5 Polarization curves for different electrical conductivity values

CHAPTER 5

CONCLUSIONS AND RECOMMENDATIONS

5.1 Conclusions

A three-dimensional SOFC model has been formulated and numerical methods have been applied to solve this model. This SOFC model includes the current collectors, gas channels, gas diffusion electrodes and catalyst layer. The single unit solid oxide fuel cell with rectangular channel is modeled for the simultaneously occurring hydrodynamics, heat transfer, multi-species diffusion, and electrochemical reaction within it.

This model is validated in the single channel fuel cell case by comparing the numerical results of current density with published data in the literature. The obtained numerical results are in good agreement with the available published data. All the validated parameters are then applied to the single unit solid oxide fuel cell. Simulations were performed for different interconnect designs which vary with the percentage contact of the interconnector rib with the electrodes. From the results 60% interconnect contact surface is considered to have better performance under the same operating conditions. A parametric study is carried out by varying the mass flow rate, hydraulic diameter and material conductivity.

The conclusions pertaining to the present thesis work are summarized below:

- The SOFC interconnect design is optimized to have better performance and stability of the fuel cell. Among the different interconnect design simulations for 25% interconnect contact area to be the design criteria with maximum temperature limit, 60% interconnect design has the better electrical performance

and considerable temperature gradient for the long life of the materials. This optimization is carried out having a good proportion between the electrical performance and temperature gradient.

- At an operating voltage of 0.6 V, the optimized 60% interconnect design has a current density and power density of 4723.85 A/m^2 and 2834.31 W/m^2, respectively and temperature gradient of 37 K along the total length of the channel.
- A parametric study is carried out by varying the fuel mass flow, hydraulic diameter and interconnects material conductivity for the optimized 60% interconnect contact design.
- At different fuel mass flow rates for anode gas channel, even if the velocity is doubled from 0.4 m/s to 0.8 m/s there is only 0.66% decrease in the power output. So, velocity at 0.4 m/s is kept constant for further simulations. Also, the mass fraction of hydrogen increased with the increasing velocity.
- Simulations were performed for different hydraulic diameters D_H =1 mm, D_H =1.23 mm and D_H =1.5 mm. For an increase in the hydraulic diameter from D_H =1 mm to D_H =1.5 mm there is 1.4% decrease in the power output. It follows that there is a decrease in the power density for an increase in the hydraulic diameter.
- Electrical conductivity of the interconnect material for SOFC should be reasonably high to have less resistance for the electron transfer. Simulations were performed for electrical conductivities Ks=4500 S/m, Ks=5000 S/m and Ks=5500

S/m. The electrical performance improves with an increase in the electrical conductivity values.

5.2 Recommendations

Fuel cell structural design and operating parameters directly influence the fuel cell performance. Most of these parameters are coupled and related to each other, such as the flow rates, hydraulic diameter, operating pressure, fuel cell temperature and diffusivity, etc. Further parametric studies such as with different mass fraction of the species, different material properties, etc., are needed to obtain the optimized fuel cell performance. As a SOFC runs at very high temperatures, the material stress analysis has to be considered. Due to its high temperature a variety of fuels can be used in the SOFC which can even produce high power densities. Further experimental investigations have to be developed to design the best interconnect for better electrical performance and high stability of the fuel cell.

REFERENCES

[1] Ryan O'Hayre, Suk-Won Cha, Whitney Colella, Fritz B.Prinz, "Fuel Cell Fundamentals" John Wiley & Sons, ISBN 978-0-470-25843-9 (2009)

[2] www.fuelcells.org

[3] www.prlog.org (Latest press release on fuel cells)

[4] www.fuelcellsworks.com

[5] Minh, Nguyen Q. "Ceramic Fuel Cells"
(1993) Journal of the American Ceramic Society, 76 (3), pp. 563-588.

[6] Yamamoto O. "Solid Oxide Fuel Cells:Fundamental Aspects and Prospects" Electrochimica Acta Volume 45, Issues 15-16, 3 May 2000, Pages 2423-2435

[7] Wilson, J. R., Gameiro, M., Mischaikow, K., Kalies, W., Voorhees, P. W., and Barnett, S. A., "Three-Dimensional Analysis of Solid Oxide Fuel Cell Ni-YSZ Anode Interconnectivity". Microscopy and Microanalysis 15, 71-77 (2009).

[8] Paola Costamagna, Paolo Costa and Vincenzo Antonuccib "Micro-Modelling of Solid Oxide Fuel Cell Electrodes" Electrochimica Acta, Vol. 43, Nos 3-4. pp. 375-394, 1998

[9] Yakabe.H, T. Ogiwara, M. Hishinuma, I. Yasuda "3D Model Calculation for Planar SOFC" Journal of Power Sources 102 (2001) 144-154

[10] Thom,F., Lehnert,W., Meusinger,J "Modeling of Gas Transport Phenomena in SOFC Anode" Journal of Power Sources Volume 87, Issue 1, April 2000, Pages 57-63

[11] Apfel. H, M. Rzepka, H. Tu, U. Stimming "Thermal Start-up Behavior and Thermal Management of SOFC's" Journal of Power Sources 154 (2006) 370–378

[12] Zijing Lin, J.W. Stevenson, M.A.Khaleel "The Effect of Interconnect Rib Size on the Fuel Cell Concentration Polarization in Planar SOFCs" Journal of Power Sources 117 (2003) 92-97

[13] Grondin. D, Jonathan.D, Mohsine.Z "Optimization of SOFC Interconnect Design Using Multiphysics Computation" 18th European symposium on Computer Aided Process Engineering (2008)

[14] Chan S.H, K.A. Khor, Z.T. Xia "A Complete Polarization Model of a Solid Oxide Fuel Cell and its Sensitivity to the Change of Cell Component Thickness" Journal of Power Sources 93 (2001) 130-140

[15] Lehnert W , J. Meusinger , F. Thom “Modeling of Gas Transport Phenomena in SOFC Anodes” Journal of Power Sources 87_2000.57–63

[16] Mitsunori Iwata , Takeshi Hikosaka , Makoto Morit, Toru Iwanari , Kohei Ito , Kazuo Onda, Yoshimi Esaki, Yoshinori Sakaki, Susumu Nagata “Performance Analysis of Planar-type Unit SOFC Considering Current and Temperature Distributions” Solid State Ionics 132 (2000) 297–308

[17] Yakabe. H, T. Sakurai “3D Simulation on the Current Path in Planar SOFCs” Solid State Ionics 174 (2004) 295–302

[18] Inui Y , N. Ito, T. Nakajima, A. Urata “Analytical Investigation on Cell Temperature Control Method of Planar Solid Oxide Fuel Cell” Energy Conversion and Management 47 (2006) 2319–2328

[19] T. Tanaka, Y. Inui , A. Urata, T. Kanno” Three-Dimensional Analysis of Planar Solid Oxide Fuel Cell Stack Considering Radiation” Energy Conversion and Management 48 (2007) 1491–1498

[20] Vinod M. Janardhanan , Vincent Heuveline , Olaf Deutschmann “Performance Analysis of a SOFC Under Direct Internal Reforming Conditions” Journal of Power Sources 172 (2007) 296–307

[21] Guilan Wang , Yunzhen Yang , Haiou Zhang , Weisheng Xia “3-D Model of Thermo-Fluid and Electrochemical for Planar SOFC” Journal of Power Sources 167 (2007) 398–405

[22] David L. Damm, Andrei G. Fedorov “Reduced-order Transient Thermal Modeling for SOFC Heating and Cooling” Journal of Power Sources 159 (2006) 956–967

[23] Thinh X. Hoa, Pawel Kosinski, Alex C. Hoffmann, Arild Vik “Numerical Modeling of Solid Oxide Fuel Cells” Chemical Engineering Science 63 (2008) 5356 – 5365

[24] Luca Andreassia, Giampiero Rubeoa, Stefano Ubertinia, Piero Lunghic, Roberto Boveb, “Experimental and Numerical Analysis of a Radial Fow Solid Oxide Fuel Cell” International Journal of Hydrogen Energy 32 (2007) 4559 – 4574

[25] Achenbach. E “Three-Dimensional and Time-Dependent Simulation of a Planar Solid Oxide Fuel Cell Stack” Journal of Power Sources, 49 (1994) 333-348

[26] Huang C.M, S.S. Shy, C.H. Lee “On Flow Uniformity in Various Interconnects and its Influence to Cell Performance of Planar SOFC” Journal of Power Sources 183 (2008) 205–213

[27] Recknagle K.P, R.E. Williford, L.A. Chick, D.R. Rector, M.A. Khaleel “Three-Dimensional Thermo-Fluid Electrochemical Modeling of Planar SOFC Stacks” Journal of Power Sources 113 (2003) 109-114

[28] Kai W. Bedringas, Ivar S. Ertesvag, Stale Byggstoyl and Bjorn F. Magnussen “Exergy Analysis of Solid Oxide Fuel Cell System” Energy Vol. 22, No. 4, pp. 403-412, 1997.

[30] Lieh-Kwang Chiang , Hui-Chung Liu, Yao-Hua Shiu, Chien-Hsiung Lee, Ryey-Yi Lee “Thermo-Electrochemical and Thermal Stress Analysis for an Anode-Supported SOFC” Renewable Energy 33 (2008) 2580– 2588.

[31] Jinliang Yuan, Masoud Rokni, Bengt Sunden “Three-Dimensional Computational Analysis of Gas and Heat Transport Phenomena in Ducts Relevant for Anode-Supported Solid Oxide Fuel Cells” International Journal of heat and Mass transfer 46 (2003) 809-821.

[32] Chan S.H and Z.T. Xia “Polarization Effects in Electrolyte/Electrode-Supported Solid Oxide Fuel Cells” Journal of Applied Electrochemistry 32: 339–347, 2002.

[33] Huijismans J.P.P, F.P.F. Van Berkel, G.M. Christie “Intermediate Temperature SOFC- A Promise for the 21st Century” Journal of Power Source 71 (1998) 107-110.

[34] K.J. Daun, S.B. Beale, F.Liu, G.J. Smallwood “Radiation Heat Transfer in Planar SOFC” Journal of Power Sources 157 (2006) 302-310.

[35] W.Z.Zhu, S.C. Deevi “Development of Interconnect Materials for Solid Oxide Fuel Cell” Material science and engineering A348 (2003) 227-243.

VITA

Graduate College
University of Nevada, Las Vegas

Krishna C Pulagam

Local address:

1600 E. Rochelle Ave,
Las Vegas, NV, 89119

Degrees:

Bachelor of Technology, Mechanical Engineering, 2007
Acharya Nagarjuna University, India

Thesis Title: Optimization of Solid Oxide Fuel Cell Interconnect Design

Thesis Examination Committee:
Chairperson, Yitung Chen, Ph. D.
Committee Member, Robert Boehm, Ph. D.
Committee Member, Jianhu Nie, Ph. D.
Graduate College Representative, Yahia Bagzhouz, Ph. D.